SOUTH EASTERN KENYA UNIVERSITY

RADIOLOGICAL ANALYSIS OF CONSTRUCTION STONES FROM SELECTED QUARRIES IN MACHAKOS COUNTY-KENYA

JOHN ONESMUS MUTUA

I423/KIT/20007/2019

A THESIS SUBMITTED IN PARTIAL FULFILLMENT OF THE REQUIREMENTS FOR THE DEGREE OF MASTER OF SCIENCE IN PHYSICS OF SOUTH EASTERN KENYA UNIVERSITY

JUNE 2023

DECLARATION

I understand that plagiarism is an offense and I, therefore, declare that this thesis is my original work and has not been presented to any other institution for any award.

Signature: ……..

Date: ……..

JOHN ONESMUS MUTUA

I423/KIT/20007/2019

SUPERVISORS DECLARATION

This thesis has been submitted for examination with our approval as University Supervisors.

Dr. Mugambi J. Linturi

Department of Physical Sciences.

South Eastern Kenya University.

Signature……

Date……

Dr. Onesmus M. Maweu

Department of Physical Sciences.

South Eastern Kenya University.

Signature……

Date……

ACKNOWLEDGEMENT

First, I wish to thank the Almighty God for His divine protection, love, good health and a very stable open mind during the entire period of this research work.

My most sincere appreciation goes to my very able and available supervisors; Dr. Mugambi J. Linturi and Dr. Onesmus M. Maweu. I am very grateful for their unrelenting guidance towards the research topic, proposal writing, research activities and thesis development. Their positive criticism and corrections gave me the much needed open mind in the dynamic field of scientific research. I am also very thankful to my lecturers Dr. Martin Riara and Dr. Fred W. Masinde (now at Kabianga University) for their inspirational insights in the wider physics discipline during my theoretical study.

I am dearly grateful to the staff in the department of Physical sciences in South Eastern Kenya University for her timely information throughout my studies. The great organization and guidance during my defense sessions cannot go unmentioned, may God have favor in their endeavors.

Special thanks to my researcher colleague-Boniface Kioko, whose energy and transport resources were highly helpful during lecture attendance, sample collection and sample transportation, God bless you bro.

Much thanks to Kitui School community for the much needed understanding and encouragement during my theoretical study and research work.

Last but not the least, special thanks to the Ministry of Petroleum and Mining in the republic of Kenyan for her unconditional support in the much needed laboratory services during my sample preparations.

May God bless everyone, whose direct or indirect interaction had a positive impact in this research work.

TABLE OF CONTENTS

LIST OF TABLES

LIST OF FIGURES

LIST OF APPENDICES

ABBREVIATIONS AND ACRONYMS

UNSCEAR	United Nations Committee on Effects of Atomic Radiations
NORM	Naturally Occurring Radioactive Materials
PMT	Photomultiplier Tube
IAEA	International Atomic Energy Association
HNBRA	High Natural Background Radiation
ICRP	International Commission of Radiation Protection
USEPA	United States Environmental Protection Agency
CRM	Certified Reference Materials
DNA	Deoxyribonucleic Acid
LET	Energy Transfer
PP	Pair Production
MCA	Multichannel Analyzer
EHT	Extra-High-Tension
KNRA	Kenya Nuclear Regulatory Authority
AED	Annual Effective Dose
ADR	Annual Dose Rate
Bq/Kg	Becquerel per Kilogram
H_{ex}	External Hazard Index
H_{in}	Internal Hazard Index
mSv/y	Millisievert per Year
nGy/h	Nano Gray per Hour

ROI	Region of Interest
NaI (Ti)	Thallium Activated Sodium Iodide Detector
FWHM	Full Width at Half Maximum
CNSC	Certified Nutrition Support Clinician
WHO	World Health Organization
RPG	Radiation Protection Glossary

ABSTRACT

All living organisms continuously are exposed to radiations of natural origin which originates from comics, terrestrial (soils and rocks) and radon. This work presents the radiological studies of sample rocks in Machakos County in Kenya which her basement systems are highly dominated by Metamorphic and Igneous rocks. The radiometric analysis of rock samples from Kyasioni, Mavoloni and Kathaana quarries would provide necessary radiological data to the community. To ascertain the radiological levels of different radionuclides from quarry rocks, a total of forty-two rock samples were randomly collected from the three quarry sites. These samples were independently prepared for activity concentration measurements which was later done by use of NaI(Ti) detector. The results obtained from analysis shows that, the average activity concentration for ^{238}U, ^{232}Th and ^{40}K was 74.75 ± 3.15 Bq/Kg, 118.48 ± 1.91 Bq/Kg and 1120.35 ± 30.07 Bq/Kg from Kyasioni quarry, 63.25 ± 3.08 Bq/Kg, 81.82 ± 1.62 Bq/Kg and 1112.55 ± 30.97 Bq/Kg from Kathaana quarry while Mavoloni quarry site values were 67.00 ± 3.09 Bq/Kg, 105.52 ± 1.97 Bq/Kg and 1019.17 ± 29.79 Bq/Kg respectively. These activity concentration values, though higher than the recommended limits did not pose major radiological threat to the population because their associated radiological parameters were within management levels. The absorbed dose rate in air was 156.94 ± 3.98 nGy/hr, 126.4 ± 3.72 nGy/hr and 140.67 ± 3.99 nGy/hr from Kyasioni, Kathaana and Mavoloni quarries respectively, against a set limit of 60 nGy/hr. Additionally, the internal radiation hazard index from Kyasioni and Mavoloni quarry surpassed the set limit of unity by 0.13 and 0.01 respectively while all the other parameters were within the set limits. Kyasioni quarry reported the highest radium equivalent activity of 326.77 ± 8.37 Bq/Kg while Kathaana recorded the lowest value of 260.44 ± 7.77 Bq/Kg. The same trend was witnessed for outdoor and indoor annual effective dose (AEDR) with Kyasioni quarry reporting the highest indoor AEDR of 0.58 mSv/y while Kathaana quarry had the lowest value of 0.47 mS/y. Besides the higher activity levels for the three radionuclides, only two radiological parameter limits (absorbed dose rate and internal hazard index) were surpassed and hence the buildings materials from these quarries are radiologically safe for construction purposes.

CHAPTER ONE

INTRODUCTION

1.1 Background to the study

Radiation is energy produced after atoms undergo radioactive decay (Weber, 1988). The decay products travel from their sources in form of energy waves or energized particles. Radiation is classified as either natural (from natural sources) or Artificial (induced artificially). Further, radiation can either be ionizing or non-ionizing. Non-ionizing radiation does not have enough energy to remove electrons from atoms thus less harmful to living things (ICNIRP, 2020). Examples of non-ionizing radiation include visible light, microwaves, and radio waves. Ionizing radiation have enough energy to remove electrons from atoms leaving them ionized. Ionizing radiation can cause harmful effects to most living things by damaging their tissue and altering their Deoxyribonucleic acid (DNA) (Karbownik & Reiter, 2000). Examples of ionizing radiation are X-rays, Gamma rays, alpha particles, cosmic rays from space, and Beta particles (IAEA, 2004).

All living organisms are continuously exposed to radiation of natural origin, which contributes to most of the effective dose equivalent they receive. Thus, ionizing radiation of natural origin is a prime public subject of discussion since it accounts for about 89% of the total exposure to human beings (UNSCEAR, 2017). Our immediate environment - air, soil, water, rocks, and plants, is extraordinarily rich in radionuclides. The concentration of these radionuclides differs from place to place. Radionuclides ^{238}U, ^{232}Th, and ^{40}K are concentrated in volcanic geographical regions and rocks characterized by phosphates, granites, and salt contents. As natural processes such as weathering rocks take place, these radionuclides find their way to the soils, water and to the plants. This process may be catalyzed by rainfalls since water flow rapidly escorts these nuclides to different places (UNSCEAR, 2017).

In rocks, the background radiation is mostly from ^{226}Ra, ^{232}Th and ^{40}K. ^{226}Ra is part of ^{238}U decay series. A number of studies have shown that radionuclides' concentration in rocks and soils and external exposure as a result of the gamma radiations not only depends on

geological but also geographical conditions and its' levels vary in different parts of the world (Dodson, 1953, Mulwa *et al.*, 2012).

Mostly, the main focus on radioactivity is the artificial sources especially from the nuclear plants, however, the utmost exposure to the population is from natural radiation sources as shown in Figure 1.1.

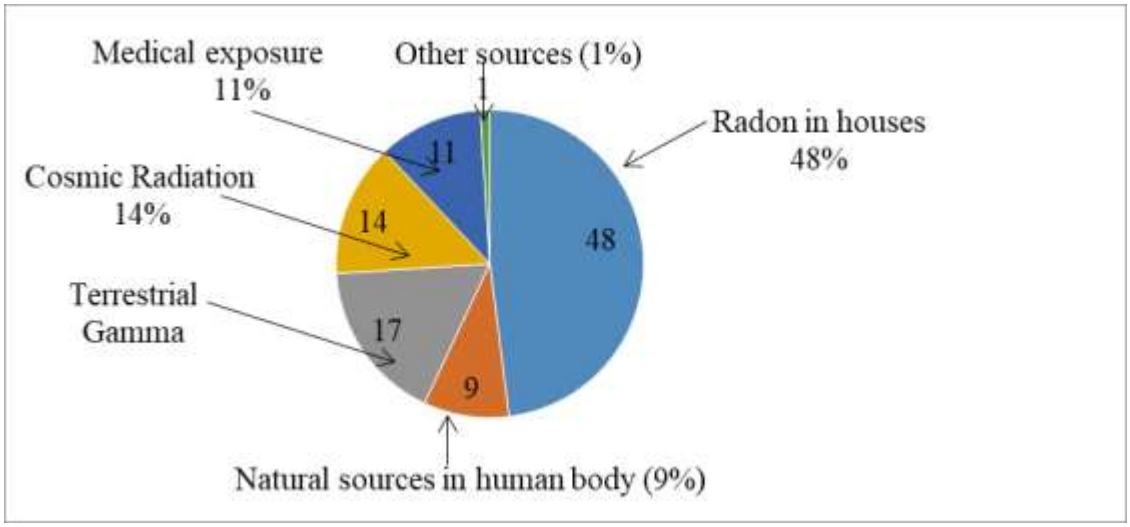

Figure 1.1: Percentage contribution of ionizing radiation to human beings by various sources (Vanmarcke, 2002).

Cosmic rays (radiation), which accounts for about 14% of the total ionizing radiation to population as shown in Figure 1.1, are defined as high-energy photons and atomic nuclei and travel through space at the speed of light ($3x10^8\ m/s$). These rays originate from solar cosmic radiation and galactic cosmic radiation and they are shielded from reaching the surface of the Earth by Earths' magnetic field and the atmosphere (Heinrich *et al.*, 1999). However, part of it penetrates these barriers and reaches the surface of the Earth. This radiation creates no harm to human beings because it is of low energy. On average, the exposure is around 3.5 millisieverts of radiation per year (Bobbo *et al.*, 2019).

Terrestrial gamma radiations come from the Earths' crust where they are mainly produced by natural deposits of Uranium, Thorium and Potassium (primordial radionuclides). While in their natural decay, these radionuclides release small amounts of ionizing radiation. Consequently, traces of these minerals are also found in building materials such as construction stones and therefore exposure to natural radiations can occur indoors as well

as outdoors. However, it is reported that radon does not significantly contribute towards outdoor radiation (Kavasi *et al*., 2010).

Radon (^{222}Rn) and Thoron (^{220}Rn) gases inhalation leads to the highest exposure of the natural origin (Kumar *et al*., 2017). Both Radon and Thoron are products of radioactive minerals found in soil and bedrock. Radon gas is part of ^{238}U decay series. It is an inert gas, a property that makes it filter up through the ground into the atmosphere with a lot of ease. Thoron is also a radioactive gas coming from ^{232}Th decay series (Kaur *et al*., 2021). In the atmosphere, the two gases are diluted to harmless levels, although they may be trapped and accumulate inside buildings to dangerous levels and hence maybe inhaled by the occupants causing health problems. Uranium miners are also at risk of exposure to radon gas which is the largest source of external exposure to human beings (Mahur *et al.*, 2008).

The human body can also suffer from internal natural exposure (ingestion). This may arise from food staffs and drinking water as they possess traces of amounts of radioactive minerals. For example, cultivation of vegetables from soil and groundwater that contains radioactive minerals would surely be rich in primordial radionuclides. On ingestion, these minerals lead to internal exposure (Brynjolfsson, 2002). Table 1.1 gives the amount of radioactivity from potassium contained in about five hundred grams of different food substances.

Table 1.1: ^{40}K content in food (Brodsky, 1978)

Food	Becquerel (Bq) per 500 grams
Red meat	56
Carrot	63
White potato	63
Banana	65
Lima bean	86
Brazil nut	103

The human body also contains various radioactive isotopes as shown in Table 1.2.

Table 1.2: Radioactive isotopes in the body (Per 70 Kg adult)

Isotope	Amount of radiation	Reference
^{238}U	2.3	Eisenbud & Gesell, 1997
^{232}Th	0.21	Eisenbud & Gesell, 1997
^{40}K	4000	Eisenbud & Gesell, 1997
^{226}Ra	1.1	Eisenbud & Gesell, 1997
^{14}C	3700	Eisenbud & Gesell, 1997
^{3}H	23	UNSCEAR, 2017
^{84}Po	40	Paquet *et al*., 2017

This study focuses on the natural radioactivity concentrations of ^{238}U, ^{232}Th, and ^{40}K in construction stones from the three selected quarries in Machakos County, which are the sources of construction stones in the expansive Machakos County and beyond. The dosimetric quantities are examined to determine the biological effect of the rising radiation energy from the three radionuclides.

1.2 Radioactive Emissions

The process of radioactive decay is accompanied by release of three ionizing radiations namely: gamma rays, beta particles, and alpha particles (Siegbahn, 2012). Gamma radiation is an electromagnetic radiation coming from the radioactive decay of atomic nuclei. It consists of the shortest wavelength electromagnetic waves, hence, giving the highest photon energy. Gamma decay includes the release of radiated gamma rays and two electromagnetic processes namely internal conversion and internal pair production. In internal conversion, excess energy in a nucleus is directly transferred to one of its orbiting electrons, which leads to the ejection of the electron from the atom (Crouthamel *et al*., 2012). In the case of internal pair production, excess energy is directly converted within the electromagnetic field of a nucleus into an electron and a positron that are emitted together. Gamma-ray photons ionize matter indirectly since they do not have an electrical charge. The ionization occurs by formerly triggering photoelectric absorption followed by Compton scattering or through pair production. Gamma rays accompany beta decay since beta decays produce excited daughter nuclides. These produced atoms attain stability by emission of gamma photon(s) as shown in Figure 1.2.

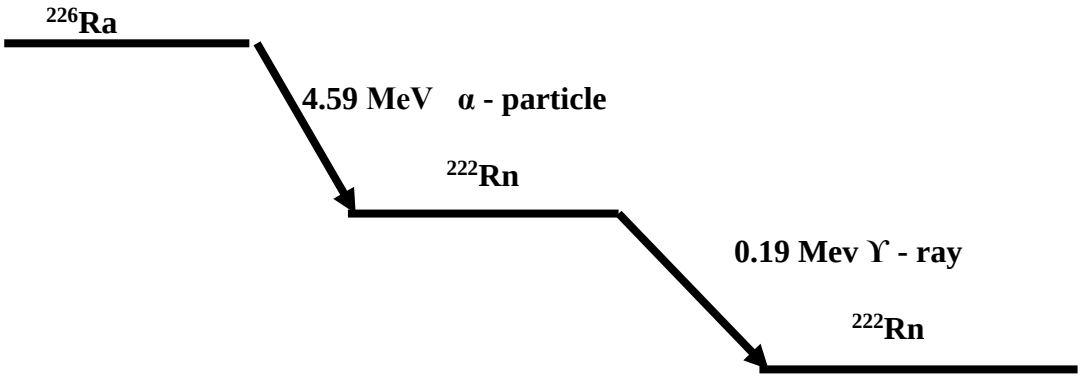

Figure 1.2: The decay scheme of ^{226}Ra (Knipp & Uhlenbeck, 1936).

1.3 Radiation limits

Radiation energy at elevated levels is harmful to human beings and therefore bodies dealing with research on radiation energy have a responsibility of advising on the safety dosimetric radiation limits. Table 1.3 shows the acceptable dosimetric limits as advised by the corresponding relevant bodies.

Table 1.3: Radiation parameter limits

PARAMETER	LIMIT	BODY
Radium equivalent	<370 Bq/Kg	(UNSCEAR, 2000)
Absorbed dose rate	<60 nGy/h	(UNSCEAR, 2010)
Annual effective dose	<1.2 Sv/y	(Valentin, 2007).
Internal hazard index	<1 Sv/y	(Podgorsak, 2005)
External hazard index	<1 Sv/y	(Podgorsak, 2005)

Construction stones contain radioactive nuclides since they originate from the Earth's crust, which has some percentage of radionuclides ^{238}U, ^{232}Th and ^{40}K. However, the radioactivity levels of the perceived radionuclides are not known. This poses a health risk to the quarry workers and the house occupants in the event these construction stones possess radionuclides whose radioactivity levels surpass the recommended limits. It is, therefore, important to measure the radioactivity concentrations of ^{238}U, ^{232}Th and ^{40}K in rocks from the selected sources in Machakos County.

1.4 Statement of research problem

The communities living in the proximity of quarry sites consider mining as their main economic activity. This exercise is widely carried out without due diligence to the geological, geographical location, ecological and chemical factors. However, all rocks contain traces of radioactive nuclides and therefore it is important to ascertain to what extend is the quarry construction stones radioactive so as to advice the quarry workers and the immediate community accordingly.

1.5 Objectives of the study

1.5.1 General objective

To determine the natural radioactivity levels of construction stones from Kyasioni, Mavoloni and Kathaana quarries.

1.5.2 Specific objectives

i. To measure the radiometric parameters of the samples.
ii. To determine the hazards indices of the samples.
iii. To compare the results from this study with findings from other related studies.

1.6 Research questions

i. What are the radiometric parameters from the selected samples?
ii. What are the hazard indices of the selected samples?
iii. How do the results from this study compare with findings from other related studies?

1.7 Justification of the study

Natural radioactivity levels are mainly determined by the geological composition of the area. Metamorphic and igneous rocks, which possess radionuclides such as Uranium, Thorium and Potassium are dominant in Machakos County (Dodson, 1953). It is, therefore, important to investigate the radioactivity levels of construction stones from the three main quarries in Machakos County namely, Kyasioni, Mavoloni and Kathaana, which are sources of construction stones in the county and its environs. In addition, this study is significant since no other radiological study that been conducted on these selected quarries

despite their major contribution in the construction industry. Furthermore, the expected radiological data from this study will go a long way in improving the radioactivity database for the country and it will also form the basis for further studies, policymaking, and regional radiological area mapping.

1.8 Scope of the study

This study covered three areas of interest namely Kathaana, Kyasioni and Mavoloni quarry sites. Kathaana quarry is in Kangundo Sub County while both Kyasioni and Mavoloni are found in Yatta Sub County, Machakos County.

A total of forty-two stone samples were randomly collected from the three quarry sites. The samples were subjected to radiological measurements through gamma-ray spectroscopy system. The counting time for each sample was eight hours (28800 seconds), and the arising spectrum was analyzed with the emerging qualitative data been the basis for activity calculation. Other radiological parameters (hazard indices and dose rates) were calculated from the mean activities of each quarry site. Statistical analysis and radiological comparison among the quarries was also done.

The main aim of this research was to determine the radiological safety of construction stone materials from the three selected quarries in terms of specific activity concentration of ^{226}Ra, ^{232}Th, and ^{40}K. For this reason, the calculation of dose rates and hazard indices focused on the average activity concentration of these terrestrial radionuclides. Their numerical calculations were determined and in-depth statistical analysis presented in chapter five.

1.9 Assumptions

It was assumed that:

i. the collected stone samples were a representation of each rock in the quarry site.

ii. there is no seasonal effects in the perceived radionuclide concentration.

iii. the concentrations of the radionuclides of interest does not vary with depth.

CHAPTER TWO

LITERATURE REVIEW

In this chapter, a review of related studies in Kenya and the world is reported. Keen attention is paid to activity concentrations from building materials as reported in various studies. Researchers from all over the globe have been undertaking research on soil samples, rock samples, and other construction materials to determine their natural radioactivity levels which may inform their suitability in the ever-growing construction industry. These studies are discussed in sections 2.1 and 2.2 for the world and Kenya, respectively.

2.1 Radiometric Surveys across the world.

Across the world, research on radioactivity levels from natural rocks, soil samples, and other related materials has been conducted and radioactivity levels of varying magnitude reported. The variation of these activity levels depends on factors such as geological, geographical location, ecological and chemical factors (El-Gamal *et al.*, 2007). These studies have mostly concentrated on human attractive sites such as mining sites, sandy beaches (Liu & Lin, 2018), rivers, groundwater (Almeida *et al.*, 2004) and rocky sites. Further, radiometric studies have also been conducted on human-dwelling areas (Enoh *et al.*, 2022). Well-documented findings of these studies have been used to adequately advise the general public on permanent settlement areas and the right protective gear in case of visiting or working in a highly radioactive environment.

Hameed *et al*., (2012), reported results of activity concentrations of primordial radionuclides from sample stones of sedimentary and igneous rocks that supply stones for the construction of buildings in Tiruchirappalli district, Tami Nadu, India. Sedimentary rocks posted a mean activity concentration of 5.4, 12.4, and 372.8 Bq/Kg for ^{238}U, ^{232}Th, and ^{40}K respectively while in igneous rocks, the concentration for ^{238}U, ^{232}Th, and ^{40}K was reported as 15.5, 135.0 and 859.4 Bq/Kg respectively. A quick comparison of the two rocks shows that igneous rocks had a higher activity concentration. The sedimentary sample rocks recorded a mean radium equivalent activity of 32.8 Bq/Kg whereas that of igneous rocks was 278 Bq/Kg and hence both findings were below the world's limit of 370 Bq/Kg, however Narthamalai sample (S13) gave a value of 689.3 Bq/Kg. Igneous rock samples

gave a mean annual effective dose of 124.5 nGy/h which exceeded the recommended limit of 60 nGy/h. The mean annual effective dose from both sedimentary (0.089 mSv/y) and igneous rocks (0.63 mSv/y) were below the 1 mSv/y recommended limit except for Narthamalai (S13) whose value was 1.48 mSv/y. This study gave the analyzed stones a radiological clean bill of health as construction materials except for ingenious rock from Narthamalai (S13).

Harb, *et al*., (2012), measured the activity concentration of ^{226}Ra, ^{232}Th, and ^{40}K in a variety of rocks using NaI(Ti) spectrometer in Giza City- Egypt. It was found out that, the activity concentration for ^{226}Ra, was 99 Bq/kg, 134 Bq/kg, and 3382 Bq/kg for gneiss, granite, and basalt rocks in that order. Further, ^{232}Th activity concentration of 211.6 Bq/kg, 170.5 Bq/kg, and 2344 Bq/kg for gneiss, granite and Basalt rocks respectively were reported. The activity concentrations of ^{40}K were 106 Bq/kg, 104 Bq/kg and 755 Bq/kg in gneiss, granite, and basalt rocks respectively. Other parameters associated with ionizing radiations from natural radionuclides were also calculated to determine the suitability of these rocks as construction materials. However, there was no significant harmful effect reported since the dosimetric parameters were within the recommended values (Valentin, 2002).

In Nigeria, Joshua *et al*., (2009), using gamma-ray spectrometry examined the activity concentrations for a wider range of rocks. From this study, Joshua reported granitic rock as having a maximum activity concentration of 882 ± 298 Bq/kg for ^{40}K. This high concentration was pegged on the high silica content and as well as little high activity concentrations for both ^{232}Th and ^{238}U, which had the values of 131 ± 43 Bq/kg and 1293 ± 8 Bq/kg respectively. The least activity concentration was reported from ferrogeneisis shale rocks for both ^{232}Th and ^{238}U radionuclides. This was attributed to low levels of iron content in this type of rock. This study concluded that these stones were radiologically safe as construction materials since all the evaluated radiological parameters did not surpass recommended.

Mbuzukongira, (2006), analyzed coltan (short form for columbite-tantalite and known industrially as tantalite) samples from the Eastern Democratic Republic of Congo. Gamma-ray spectrometry was used in the measurement of activity concentration for both ^{226}Ra and ^{232}Th. The measurement of the coltan samples was done for 72000 seconds and ^{40}K could not be detected, however, through calculation, its value was found to be 0.141 Bq/g. Further

this study reported that all the coltan samples had radiation activity concentrations for ^{226}Ra in the range of 0.32 to 1.56 Bq/g. These concentrations were high when compared to the concentrations gotten from typical soil and rock samples which was 0.01 to 0.05 Bq/g and 0.007 to 0.05 Bq/g for ^{226}Ra and ^{232}Th respectively. The determined effective dose and total dose to the miner had values that differed by a range of 0.007 to 18.1 mSv/y based on the work activity performed by each artisan.

The measurement of natural radioactivity levels in the sandy beaches of Quarapari state of Brazil reported activity concentration in the ranges of (6 to 4100) Bq/kg, (20 to 5700) Bq/kg, (17 to 47500) Bq/kg, and (73 to 3000) Bq/kg for ^{226}Ra, ^{214}Pb, ^{232}Th and ^{40}K respectively (Veiga *et al.*, 2006). In the Areia Preta region, the reported findings showed that the level of ^{232}Th and ^{40}K was above the corresponding global mean. The absorbed dose rate in this area was reported to be in the region of 18 to 37500 nGy/h with a mean value of 18518 nGy/h which was above the world's permissible limit of 60 nGy/h from primordial radiation and the world. The concentration of ^{232}Th from this beach was reported to be more than the concentrations from other beaches of coastal Brazil. The measurements from these studies were done using gamma-ray spectrometry, (Alencar & Freitas, 2005).

Lakshmi *et al.*, (2005), measured the natural activity levels in sand from Tamilnadu beach in the North East of India using NaI(Ti) detector. His main interest was to evaluate the radiation hazards from the radioisotopes of ^{232}U, ^{232}Th, and ^{40}K which he reported to be in the range of (below detectable limit to 254) Bq/kg, 13 to 3576 Bq/kg and (15 to 524) Bq/kg respectively. In addition, this study reported a mean radium equivalent of 1081.86 Bq/kg which was way beyond the permissible limit of 370 Bq/kg (UNSCEAR, 2017). Further, the average absorbed dose rate came close to eight times the world's average of 60 nGy/h as it stood at 504.75 nGy/h. This was attributed to Monazite deposits in the sand samples. External hazard indices reported a mean of 2.91 mSv/y and hence surpassing the recommended limit of 1 mSv/y (Clarke, 1992) by 1.91 mSv/y while a mean of 0.621 mSv/y for annual effective dose rate was reported. Based on the elevated levels of the reported radiometric parameters, this study concluded that the beach possessed enhanced natural radioactivity levels and therefore posed a radiological health threat to the people visiting and interacting with it.

Sohrabi, (1998) in Yangjiang, China, reported an elevated level of radiation energy from both ^{232}Th and ^{238}U radionuclides in surface soil and construction materials by the use of gamma-ray spectrometry. Further, this study reported an external average dose of 2.1 mSv, a mean annual effective dose of 6.4 mSv, and an internal dose of 4.3 mSv - all above the recommended limits.

Sohrabi, (1993), reported activity concentrations of 86400, 187, and 1380 Bq/kg for ^{238}U, ^{232}Th, and ^{40}K respectively in Ramsar, a northern coastal city in Iran. These concentrations were higher than the world's average of 33 Bq/kg for ^{226}Ra, 45 Bq/kg for ^{232}Th, and 420 Bq/kg for ^{40}K (UNSCEAR, 2017). Moreover, Ramser state reported the highest annual dose rate of 260 mSv/y (Ghiassi-Nejad *et al*., 2002) which was the highest annual dose rate and could be attributed to high radium in deposits from hot springs while thorium concentration would be due to travertine deposits.

2.2 Radiometric surveys in Kenya

Radiometric studies in Kenya have been conducted with a view of determining the natural radioactivity levels and evaluating the associated radiological parameters from some regions, rocks, soil, and other materials. These studies have reported different mean indices and ranges for various dosimetric quantities. The reports from some of these studies are as follows.

Matsitsi *et al*., (2019), examined the activity levels from sand and rock samples in Tyaa River, Kitui County using HPGe gamma-ray spectrometry. This study reported activity concentrations of 33 Bg/Kg, 55 Bg/Kg, and 812 Bq/Kg for ^{226}Ra, ^{232}Th, and ^{40}K respectively from sand samples. From rock samples, the concentration was reported as 21 Bq/Kg, 49 Bq/Kg, and 782 Bq/Kg for the respective radionuclides of ^{226}Ra, ^{232}Th, and ^{40}K. The mean values for the radiological hazard indices and dose rates did not surpass the ICRP recommended limits and hence this study concluded that the examined materials had no biological harm when used for construction purposes.

Kinyua *et al*., (2011), did a radiological survey using gamma-ray spectrometry on five major soapstone quarries in Kisii County. This study reported that the concentrations of the radionuclides of ^{232}Th ^{226}Ra and ^{40}K were in the range of 38.6 to 271.7 Bq/kg, 43.1 to 360 Bq/kg, and 307 to 1780 Bq/kg respectively. The average total absorbed dose rate was reported as 177.6 nGy/h inside the quarries while the mean for absorbed dose rate, one

meter above the ground was found to be 541.4 nGy/h. Below the Earth's surface, the calculated dose rate was found to be approximately three times the world's average of 60 nGy/h. Both internal and external hazard indices surpassed the permissible limits (ICRP, 1991) for they were found to stand at 1.03 and 1.27, respectively. Therefore, considering these findings, soapstone mining from these quarries was not radiologically safe to the miners.

Mustapha *et al*., (1999), studied the activity concentrations of radionuclides in construction natural rocks and soil samples using a gamma-ray spectrometer. This study investigated external Gamma-ray energy absorbed doses and the effective dose equivalent. The activity concentrations and their corresponding conversion factors were used to determine the exposure rates from the natural radionuclides. This study reported that the effective dose ranged from 0.1 to 0.2 mSv/y from terrestrial gamma radiations, 0.4 to 0.6 mSv/y was from inhaling radon while cosmic radiation contributed a range of 0.2 to 0.7 mSv/y. Furthermore, indoor air was found to have a radon concentration of 5 to 1200 Bq/m^3 and drinking water had 1 to 410 Bq/L.

Radioactivity surveys in southwestern Kenya, precisely in several parts of Lambwe's east location have shown that the mean estimated annual external effective dose rate by radionuclides in the rocks and soils samples was 5704.78 msv/y (Otwoma *et al.*, 2013). Gamma-ray spectrometer confirmed the average specific activity concentrations of ^{40}K, ^{238}U, and ^{232}Th in the soil and rock samples to be 508.67 Bq/kg, 178.69 Bq/kg, and 1396.85 Bq/kg respectively. The presence of carbonatite rocks was said to be behind these much-elevated findings. In addition, this area reported a gamma absorbed dose rate of 5.705 mSv/y in the air which is more than the world's mean of 0.46 mSv/y (UNSCEAR, 2017). Based on these findings, this area was rendered a high natural background radiation area (HNBRA), (Achola, 2009).

X-ray fluorescence analysis of soil and rock samples from Mrima hills confirmed high concentrations of Zinc, Thorium, Lead, and Strontium (Mangala, 1987). Water samples from this region (Mrima hills) have also seen radon activity levels to be around 100 KBq/m^3 (Mustapha, 1999). This finding was attributed to the occurrences of Thorium enriched carbonates in the area.

In Kitui South, Mulwa *et al*., (2013) investigated the radiological suitability of naturally occurring limestone in that area as a construction product. The study reported activity concentration of the limestone samples and its' associated radiometric parameters as with the recommended limits. The results for all examined samples gave hazard indices below a unit and likewise no sample surpassed radium equivalent activity recommend limit of 370 Bq/kg. Based on these findings, it was concluded that limestone can be used as building material or for manufacture of building materials.

Many studies have been conducted on various natural rocks, soil, and water to ascertain their activity concentrations and hence their safety, however, no radiological research has been done on rocks from Kyasioni, Mavoloni, and Kathaana quarries despite their contributions to the supply of construction materials in the country. In this current study, NaI(Ti) detector was used in the measurement of activity radiation energy from the collected rock samples. This research aimed at bringing the necessary radiological data from these quarries on board.

CHAPTER THREE

THEORITICAL BACKGROUND

3.1 Introduction

This chapter presents a theoretical discussion around ionizing and non-ionizing radiations, interactions of radiations with the matter, biological effects of ionizing radiations, and some insights into radiation dosimetry and states of equilibrium.

3.2 Categories of Radiations

Radiations are classified into ionizing and non-ionizing radiations.

3.2.1 Ionizing Radiations

This is energy in form of particles and electromagnetic waves (Mba *et al*., 2012). The magnitude of this energy is enough to penetrate matter, knocking off electrons (from atoms and molecules) and, hence ionizing it (Andreo *et al*., 2017). Ionizing radiations include fast electrons (beta, positron), heavy charged particles (protons-hydrogen nucleus, Deuteron-its nucleus has a proton and a neutron, Triton-tritium nucleus having a proton and two neutrons, Alpha-helium nucleus with two protons and two neutrons in the nucleus), photons (gamma and x-rays) (Allen, 2011). Further, ionizing radiations are classified into either direct or indirect (Ward, 1988). The interactions due to direct ionizing radiations take place when charged particles such as electrons possessing enough kinetic energy interact directly with atoms or molecules. This process generates radicals which continue to interact with other molecules until they exhaust all their kinetic energy (Urbain, 2012). Figure 3.1 illustrates how cell damage occurs as a result of direct and indirect ionization.

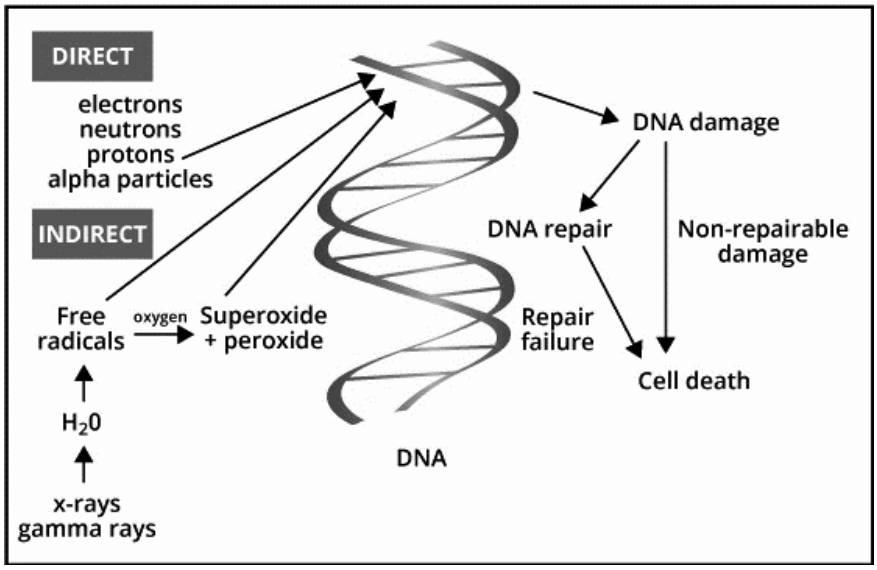

Figure 3.1: Cell damage under direct or indirect ionization (Riley, 1994)

The interaction under indirect ionization takes place in two stages: i) Photons (gamma and x-rays) interact with cellular water and the latter absorbs enough energy that makes it ionize into hydrogen ions and hydroxyl radicals. ii) These free radicals interact with cellular atoms and molecules which further leads to more formation of radicals and damage to the cells. It can be noted that free radicals have unpaired electrons in the structure which react with DNA molecules to cause molecular structural anomalies, (Valko *et al*., 2007).

3.2.2 Non-ionizing Radiations

These are radiations of less kinetic energy and therefore unable to dislodge electrons from atoms and molecules and hence not able to ionize matter. For this reason, they are less harmful to human health. The examples are radio waves, ultraviolet, infrared, visible light, and microwaves (Hietanen, 2006).

3.3 Uses of Radiations

Radiations of high penetrating power are used in medical imaging, industrial determination of gauges, sterilization of medical equipment, food irradiation, etc. Direct and indirectly ionizing radiations are used in radiotherapy, diagnostic radiology and nuclear medicine (Podgorsak, 2005). On the other hand, radiations of less energy (less penetrating power) are useful in ways such as food cooking (use of microwaves), radar communication, information transmission (radio waves), food production in greenhouses, mineral analysis, infrared photography, source of vitamin D and skin treatment (Podgorsak, 2005).

3.4 Gamma Radiation

Gamma radiations are characterized by higher energy magnitude and are produced when unstable atomic nuclei undergo a radioactive decay to attain stability (Khan & Gibbons, 2014). Gamma rays penetrate matter and the process is accompanied by release of energy. The longer distance traversed through matter is made possible by the fact that besides their high penetrating power they have zero mass (Bushberg & Boone, 2011). Due to the deep distance covered through matter, their energy distribution is low per unit area and therefore they are said to be radiations of low "linear energy transfer" (LET).

Gamma radiations are electrically neutral and therefore they indirectly ionize matter. The ionization takes place in steps; first, the interaction leads to photoelectric absorption followed by Compton scattering or pair production. The energy (E) produced by gamma rays is given by equation 3.1.

$$E = hv \qquad 3.1$$

Where h is the Plank's constant and v is the radiation frequency. If the energy of gamma radiation is less than 10 MeV, it is considered safe for human health since there is no interaction between it and the body cells (Diehl, 1999).

Besides artificial production, gamma rays are naturally released from terrestrial radionuclides and also as secondary radiations because of atmospheric interactions with cosmic ray particles (Britannica, 2021).

The emission of Beta particles produces radioactive radionuclides whose decay process is accompanied by the release of gamma rays. A good example is ^{60}Co which undergoes a radioactive decay to form a stable element (^{60}Ni).

The process produces excited Nickel particles accompanied by gamma radiations as shown in Figure 3.2.

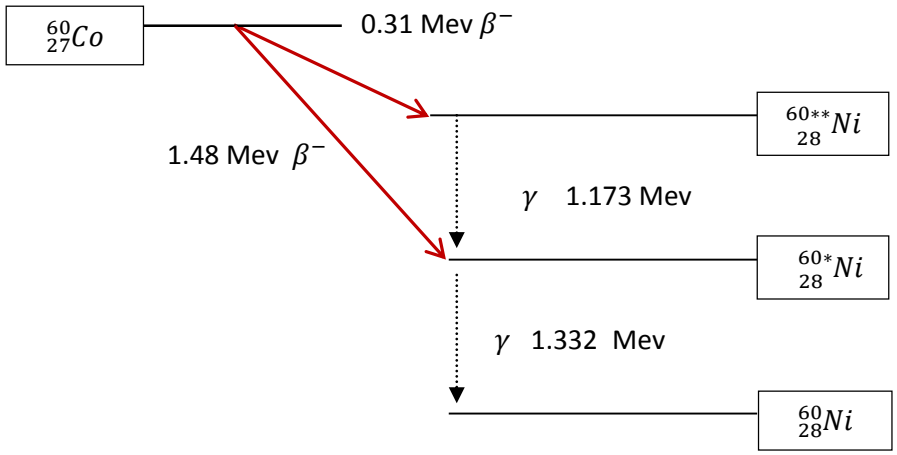

Figure 3.2: The decay scheme of ^{60}Co (Yang *et al*., 2019)

3.4.1 Gamma Radiation Interaction with Matter

The interaction between gamma radiation and matter mainly leads to i) attenuation of the radiation beam intensity ii) the gamma radiation photon may undergo total absorption and iii) the photon may be scattered by matter (Knoll, 2010). Furthermore, photonuclear reaction and coherent scattering occur in gamma-ray spectroscopy. Coherent scattering is characterized by the re-emission of radiation though in a different direction but having the same kinetic energy. This case has zero energy transfer to the detector. On the other hand, the photonuclear reaction is unlikely to occur for geological samples in most gamma-ray measurements because it needs energy of above 5 MeV (Gilmore, 2008).

The intensity (I_r) of the photon bean is given by equation 3.2

$$I_r = I_o e^{\ \mu d} \qquad 3.2$$

Where I_o is the initial radiation intensity, e is the symbol for exponent, d is depth of penetration in the body by the radiation and μ is the linear attenuation coefficient. Note that μ is defined as the probability per unit length that the photon will be removed from the beam (Knoll, 2010).

3.4.2 Photoelectric Effect

This is a case of interaction between a photon and an inner shell electron and it leads to the removal of the electron from its shell. For this effect to occur, the incident photon's energy

($E = hv$) must be greater than the binding energy (E_b) of the electron in its shell (K edge), and the electron is tightly bound in the k-shell. Once the electron has been removed (referred to as a photoelectron), the incident photon is fully absorbed, and this process creates an unstable atom. The atoms' quest for stability is quenched when an outer shell electron proceeds to fill the vacancy left in the inner shell. As this electron moves towards the inner shell, it losses part of its kinetic energy and as a result, a characteristic radiation (x-ray photon) is released (Seibert, 2004).

The kinetic energy (E_e) of the emerging photoelectron is given by equation 3.3

$$E_e = hv - E_b \qquad 3.3$$

Where hv is the incident photons' energy and E_b is the electron's binding energy. The unstable atom can also gain stability by redistribution of its excitation energy among the remaining electrons and as well another electron can be released. This process is referred to as the Auger Cascade. Figure 3.3 shows photon absorption and photoelectric emission.

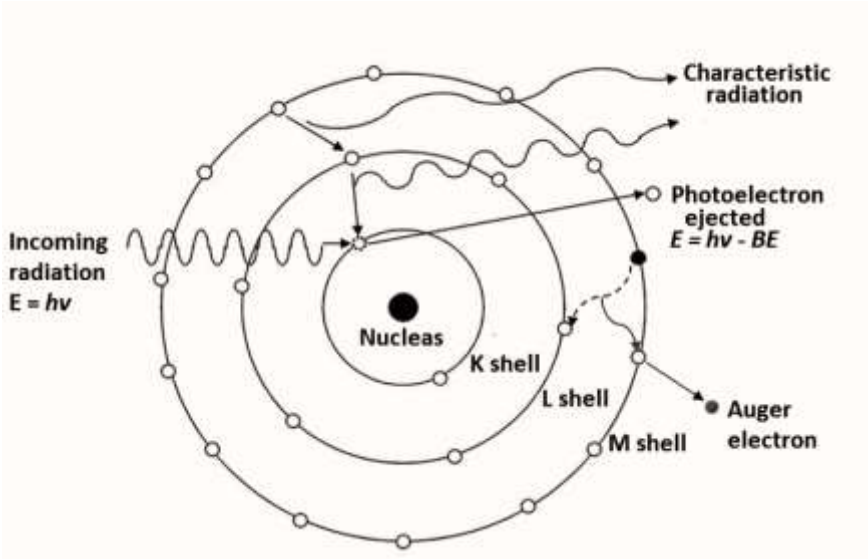

Figure 3.3: Photoelectric emission of electrons by photo-absorption of gamma radiations (Mahuvava & Du Plessis, 2015)

3.4.3 Compton Effect

Compton Effect is one of the prime forms of photon interaction and it is said to be the leading root of scattered radiation in each body. This interaction takes place between the photon and the free electrons or weakly bound valence shell (outer shell) electrons. During the interaction, the incident photon changes direction (scattered) and wavelength and loses

part of its kinetic energy to the emerging recoil electron. In this process, both energy and momentum are conserved. The energy (E_s) of the scattered photon is given by equation 3.4

$$E_S = \frac{hc}{\lambda} \qquad 3.4$$

While its momentum (P_s) can be obtained from equation 3.5

$$P_s = \frac{hv}{c} \qquad 3.5$$

Where h is the plunk's constant, c is the speed of light, v is the frequency of the photon, and $\boldsymbol{\lambda}$ is the wavelength of the radiation. The energy lost by the incident photon is referred to as the Compton shift (shift of wavelength/frequency). The photons' change in wavelength (λ) can be determined from equation 3.6

$$\lambda = 0.024(1 - \cos\theta) \qquad 3.6$$

Where θ is the scattering angle. An increase in the scattering angle decreases the energy of the scattered photon. As the scattering angle tends to zero, the scattered photon maintains its' initial energy and as a result the recoil electron receives zero energy, and for a case whereby θ = 180^0, the incident radiation photon is scattered perfectly backward and the recoil electron takes the direction of the incidence radiation (Rittersdof, 2007). Furthermore, Compton scattering is the main process during the human irradiation process, and it takes place in the energy range of 30 KeV to 30 MeV for both diagnostic and therapeutic procedures (Manohara & Hanagodimath, 2007). Figure 3.4 is an illustration of Compton scattering.

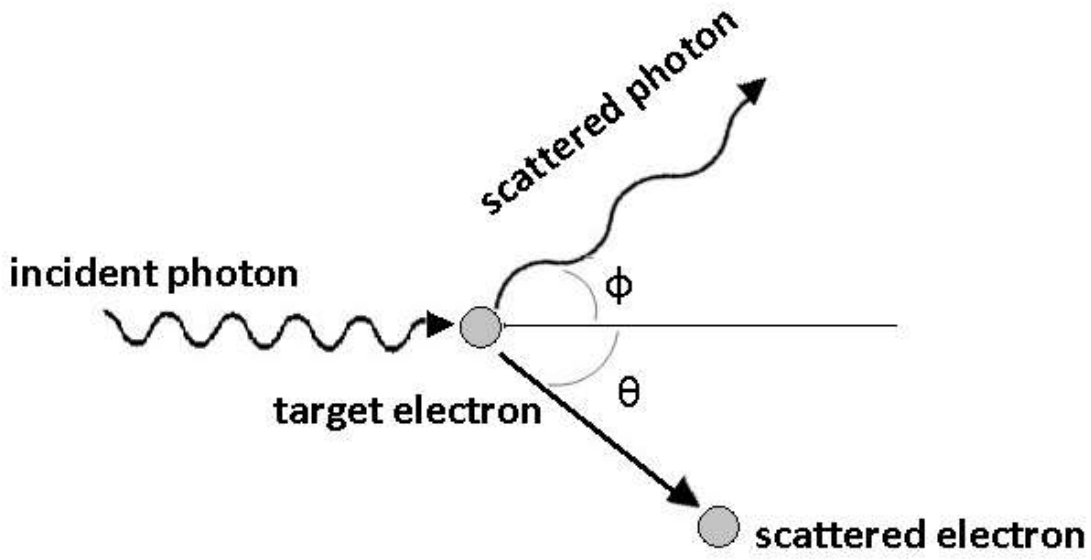

Figure 3.4: Compton Effect of an incident photon by an electron (Venugopal & Bhagdikar, 2012)

3.4.4 Pair production (PP)

In pair production (pp), there is a complete attenuation of the incident photon. In this case, pair production takes place at an incident photon energy not less than 1.022 MeV. Around the nucleus, the photon interacts with the strong electric field and as a result, it undergoes a transformation leading to the creation of two particles (a pair) namely an electron and a positron (antimatter equivalent of the electron) and hence the name pair production. The pair production is not only for electron-positron pair, other pairs may arise, notable examples include the Muon-antimuon pair and tau-antitau pair. However, these two pairs require higher incident photon energy for their formation since their resting energy masses are also high, that is 1776 MeV for tau and 105 MeV for Muon. The calculation for the rest energy masses for both electron and positron particles is determined by equation 3.7.

$$E = MC^2 \qquad 3.7$$

Which gives 0.511 MeV ($9.1x10^{-31}Kg$) for each particle and therefore the two particles give a total rest energy of 1.022 MeV. This implies that in the production of this pair, an incident photon energy greater than 1.022 MeV is needed such that the excess energy provides the two particles with the necessary kinetic energy. The photon energy above 1.022 MeV is shared between the electron and the positron (but not always shared equally) (Nelson & Reilly, 1991).

The two particles (electron and positron) are dissipated through successive interactions within the medium where the electron is quickly absorbed. The positron combines with the neighboring electron and the two neutralize one another (annihilation radiation). Through this phenomenon (annihilation radiation), both the electron and the positron are taken back into two photons (electromagnetic radiation) each having an energy of 0.511 MeV. The two are traversing the medium at 180 degrees between themselves and they end up being either absorbed or scattered in the medium. In industrial radiotherapy involving higher atomic number elements irradiation, pair production may be the main attenuation process if the incident radiation energy is more than 1.022 MeV (Michaud, 2013). An illustration of pair production is show in Figure 3.5

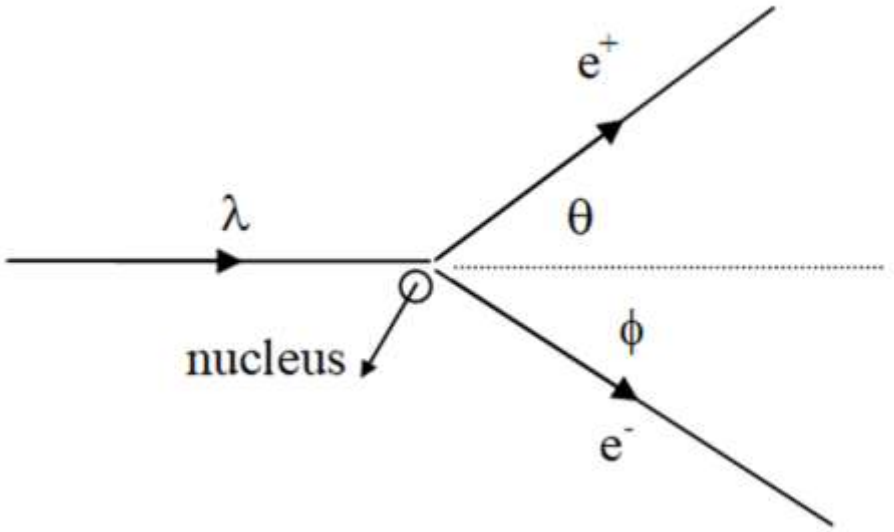

Figure 3.5: Pair production of an electron and a positron due to interaction between high energy incident photon and an atomic nucleus

3.5 Radioactive Decay Law

This law refers to the spontaneous disintegration of radioactive nuclei (Malik, & Gupta, 1989). During this process, particles such as beta and alpha are emitted accompanied by gamma photons. In an excited state, radionuclides find stability by further decay (decay chain/series) and as a result, more gamma photons are released. The disintegrating nuclide is referred to as the parent nuclide while the emerging element is known as the daughter nuclide. Further decay of the daughter nuclide takes place and the process continues until

a stable element is formed (Saha, 2004). It is important to note that radioactive decay process is not affected by factors such as pressure, temperature, and chemical composition (Kendall & Caldwell, 1998).

If activity A is considered (rate of decay) for a given radionuclide having a number N of radioactive nuclei, then from the radioactive decay law, the rate of decay (activity A) of a radioactive material at a time t is directly proportional to the number (N) of radioactive nuclei present in the material at that time, mathematically expressed as shown in equation 3.8.

$$A = \frac{dN}{dt} \alpha\ N \text{ Or } \quad A = \frac{dN}{dt} = -\lambda N \qquad 3.8$$

Where λ is the decay constant (constant of proportionality) and the negative sign denotes a decrease in activity with time.

The decay constant depends on the disintegrating radionuclide.

The solution for the number N in equation 3.8 is given by equation 3.9

$$N = N_o e^{-\lambda t} \qquad 3.9$$

Where N_o is the initial number of parent nuclei at time $t\ =\ 0$ and t is the time taken for the initial number of parent nuclei No to decay to present number N. Substituting equation 3.9 into equation 3.8, activity A, becomes:

$$A = \frac{d}{dt}\left(N_o e^{-\lambda t}\right) \qquad 3.10$$

On differentiation, equation 3.10 gives

$$A = -\lambda N_O e^{-\lambda t} \qquad 3.11$$

If we let $A_O\ = -\lambda N_O$, then equation 3.11 becomes,

$$A = A_o e^{-\lambda t} \qquad 3.12$$

Equation 3.12 shows that, the activity of a radioactive material decreases exponentially with time t (Arthur *et al*., 1981).

3.5.1 Transient Equilibrium

It is a type of equilibrium that exists at a time when half-life of the parent nucleus is longer than that of the daughter nucleus (Khan & Gibbons, 2014). A perfect example is observed in thorium decay series for the decay of ^{212}Pb to ^{212}Bi whose half-lives are 10.64 hours and 1.009 hours, respectively. The sum of parent's and daughter's activities give the total activity for the radioactive sample (Harb, 2004). Figure 3.6 gives a further illustration of transient equilibrium.

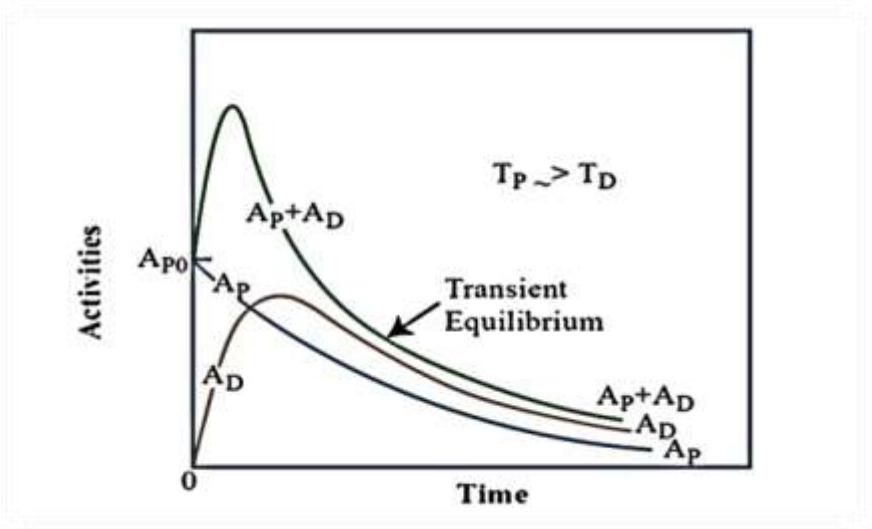

Figure 3.6: Transient equilibrium, (OCW, 2008)

3.5.2 Non-Equilibrium

This is a type of equilibrium that exists when the half-life of the parent is less than the half-life of the daughter which means that as the activity of the parent ends that of the daughter is still in existence (Gilmore, 2008). This is realized when the wavelength of the daughter particle is less than that of the parent particle. This condition holds for the transmutation of ^{218}Po at half-life of 3.10 minutes to ^{214}Pb at half-life of 26.8 minutes (Lieser, 2008). Figure 3.7 is a good illustration of Non-Equilibriun.

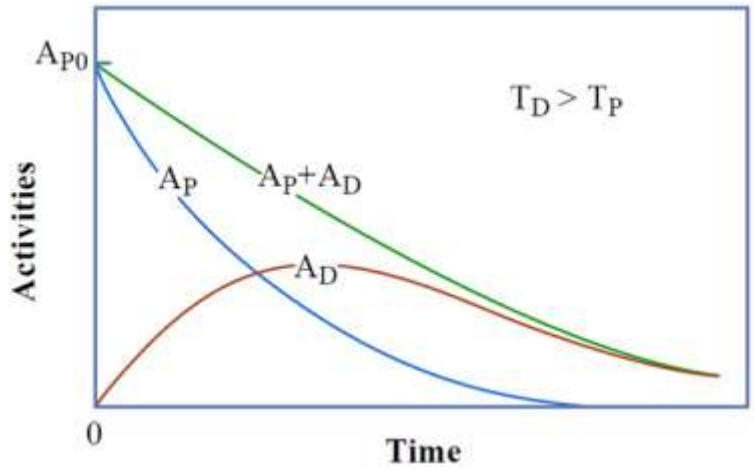

Figure 3.7: Growth and decay of a longer lived daughter (T_D) from a short lived parent (T_P) in case of no equilibrium (OCW, 2008)

3.5.3 Secular Equilibrium

Secular equilibrium occurs when both parent radionuclide and daughter radioisotopes have the same activity (same decay rate). For this type of equilibrium to exist, the parent's half-life must be greater than that of the daughters (Rösch & Knapp 2011). The decay series members experiencing secular equilibrium have the same activity. The explanation for this is that the measure of the daughter radionuclides accumulates until the number of its atoms decaying per unit time becomes equal to the number being produced per unit time (Donnelly *et al.*, 2004).

If the initial number of atoms for the parent radionuclide (N_p) and that of the daughter radionuclide (N_d) and their respective activities are considered, such that the parent radionuclide activity is represented by A_p and that of the daughter by A_d, then from the decay radioactive law, the relationship in equation 3.13 can be deduced.

$$\frac{dN_d}{d_t} = \lambda_p N_p - \lambda_d N_d \qquad 3.13$$

where λp is the decay constant for the parent radionuclide and λd is the decay constant of the daughter. Figure 3.8 shows an illustration diagram of secular equilibrium.

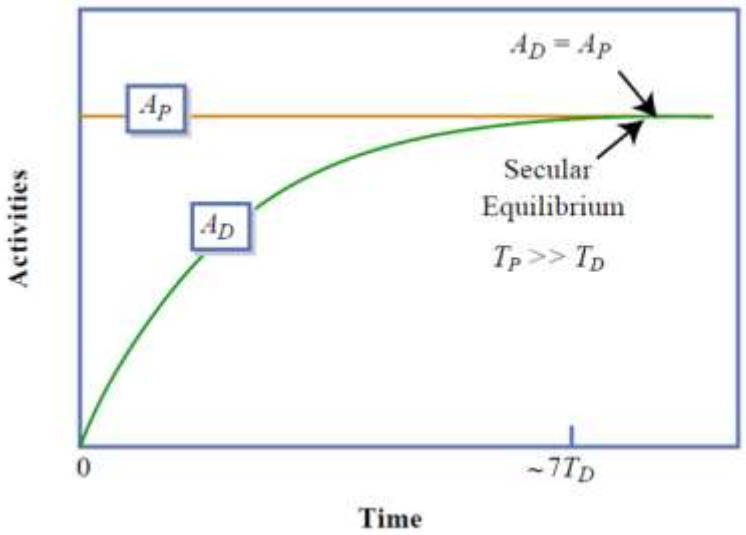

Figure 3.8: Growth of a short-lived daughter (T_D) from a much longer lived parent (T_P) until reaching Secular Equilibrium (OCW, 2008).

3.6 Radiation Dosimetry and Field Quantities

As defined by International Commission on Radiological Protection (ICRP), Effective and Equivalent dose are protection quantities. The summation of received doses (from intakes of radionuclides and external sources) gives a proper comparison with dose limits which are provided to reduce the risk of exposure effects (or the risk of hereditary and cancer effects). ICRP provides dose coefficients for the determination of internal doses because of inhalation or ingestion of radionuclides by public members, workers and even children. These dose coefficients are published as reference values and therefore they have no corresponding uncertainties which implies that, assessment of uncertainties is important in particular analysis of doses and risks and in epidemiological studies (Harrison, & Streffer, 2007).

3.6.1 Energy Fluence (Y)

This is the energy flow in a photon beam and is defined as the amount of energy dE, crossing a unit area dA(Seuntjens et al., 2005). Its SI unit is Joules per square meter. Photons release energy to electrons in two ways, first by hard and soft interactions and second by radiative interactions involving electron-positron annihilation and bremsstrahlung production (Sempau et al., 2003). These interactions are illustrated in Figure 3.9.

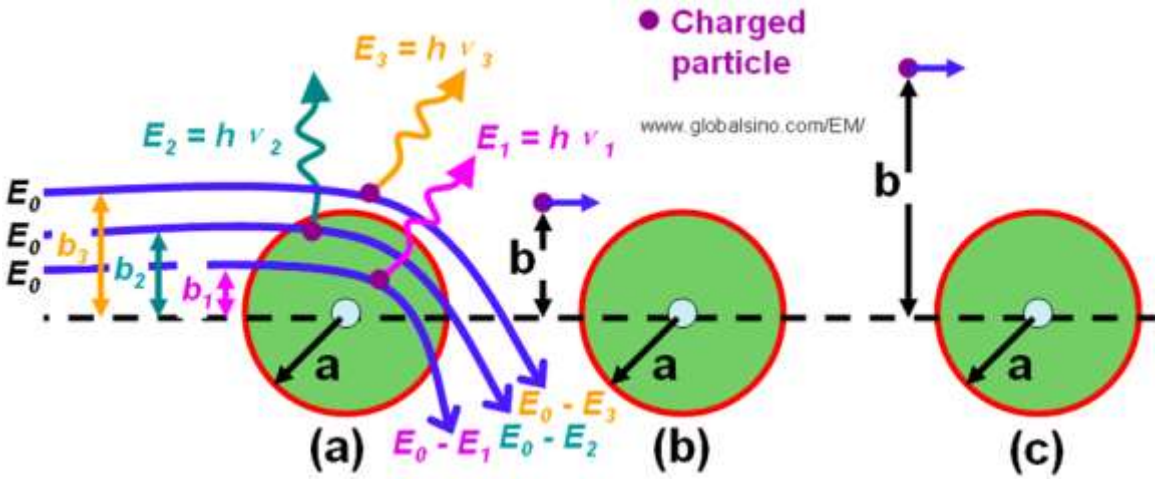

Figure 3.9: Radiative collision (a), hard collision (b) and soft collision (c) b is the impact parameter atomic radius (Liao, 2006)

As the charged particle travels through matter, it experiences coulomb interactions with the nuclei and the orbital electrons of the atoms in matter. These interactions are of three categories distinguished by the impact variable b comparable to the atomic radius a.

a) Interaction with the external nuclear field which takes place when b<<a (bremsstrahlung production)
b) Interaction with the orbital electrons for b≈a (hard collision)
c) Interaction with orbital electrons when b>>a (soft collision) (Leo, 2012).

3.6.2 Particle Fluence (ϕ)

It is the sum total of particles (gamma radiation photons) which are crossing over a spherical surface of unit cross section and surrounded by a point source of ionizing radiation (Kudriashov & Kudriashov, 2008). If the number of particles d_N crossing over a spherical surface of cross-sectional area d_A considered, then particle fluence is given by equation 3.14 (Tricot *et al*., 2013).

$$\phi = \frac{d_N}{d_A} \qquad 3.14$$

The SI unit for particle fluence is square meter. The particle fluence rate is defined as the number of particles crossing per unit time. This number of particles is numerically equal to the product of the number of particles and their average speed ((Kudriashov & Kudriashov, 2008).

3.6.3 Kinetic Energy Released Per Unit Mass (K)

This is the amount of energy that is transferred from photons to electrons per unit mass at a certain position. Its' SI unit is Gray (Joules per Kg) (Seuntjens *et al*., 2005). It can be determined from equation 3.15.

$$K = \frac{d\bar{E}_{tr}}{d_m} \qquad 3.15$$

Where $\bar{E}_{tr}$ is the mean kinetic energy transferred to charged particles from uncharged particles in mass m of the given substance. The total K (K_{total}) can be split in two parts, Collisional K_{coll} and Radiative K_{rad} and hence total K (K_{total}) is given by equation 3.16.

$$K_{total} = K_{coll} + K_{rad} \qquad 3.16$$

It is worth to note that at radiological energies, deposition and transfer of energy is virtually equal but at higher energies, a photon may interact with tissue in one position creating a photo-electron of sufficient kinetic energy and which ends up depositing this energy at a location away from the interaction point (Seuntjens *et al*., 2005).

3.6.4 Absorbed Dose (D_T)

It is the measure of energy deposited in a unit mass at a certain position. Its SI unit is the Gray (Joules per kg) (Fisher & Fahey, 2017). For a given absorbed dose, the exact value of imparted energy in a cell is the product of the frequency of energy deposition events and the value of energy deposited in each event (Valentin, 2005).

3.6.5 Equivalent Dose (H_T)

This is a measure of radiation dose to tissue and its approximation is done from absorbed dose with respect to the provided conversion factors for different body organs. Its SI unit is the Sievert (Sv) although rem is also used (1Sv = 100 rem) (McCollough & Schueler, 2000). Equivalent dose is determined from the product of absorbed dose to the organ or tissue (D_T) and the radiation weighing factor (W_R). The value of the radiation weighing factor varies in different radiations. The difference is occasioned by the type and energy of incident radiations. X-rays, gamma rays and beta particles have a W_R of 1 while that of protons and alpha particles is 2 and 20 respectively. The W_R for neutrons is between 5 and 20 depending on their energy (Schmid *et al*., 2010).

3.7 Gamma-ray spectrometry

This is an approach employed to give quantitative energy information of the spectra from gamma-ray sources. A gamma-ray energy spectrum is yield when radioactive emissions from various sources are detected and analyzed by an energy calibrated gamma-ray spectroscopy system. The energy calibration of the detector is done using specific energy peaks from standard reference sample such that every channel is assigned a specific energy value. The spectrum is important in that, from it, the identity and energy quantity of the present radionuclides can be determined. The spectrometer consists of a NaI(Ti) scintillation detector coupled with a MultiChannel Analyzer (MCA) that is used for data acquisition and storage. Its resolution is 1.33 MeV of ^{60}Co at 60 KeV and an efficiency of 7.5% at 1.33 MeV for ^{60}Co. Figure 3.10 gives a schematic diagram of the setup (Litvinenko *et al*., 2020).

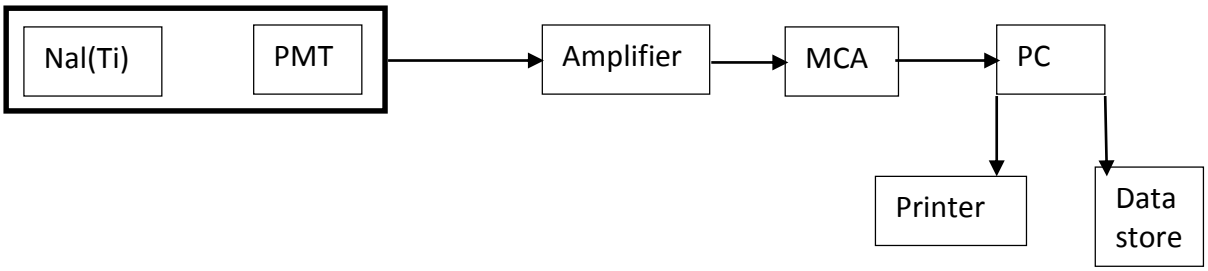

Figure 3.10: Schematic diagram for scintillation gamma-ray spectrometer system

3.8 Working of NaI(Ti)–Gamma Ray Spectrometer

NaI(Ti) detector model VG-BB-98/6D1 coupled with a PhotoMultiplier Tube (PMT) was used for gamma radiation measurement. This system is composed of a MultiChannel Analyzer (MCA) detector, amplifier/extra-high-tension (EHT) power, and a Personal Computer (PC). From the source, gamma rays make their way to the detectors' crystals and interact with the atoms of the crystals. This interaction results in the ionization of particles, which releases their kinetic energy by exciting and ionizing atoms in the crystals. The excited atoms return to the ground state by emission of light. The emitted light pulses hit the photocathode of the PMT and electrons are ejected from the cathode (Lecoq, 2020).

Amplifier/Extra-high-tension (E.H.T)-the ejected electrons are accelerated to a dynode (second electrode) whose potential is positive and higher than that of the photocathode.

Each electrode striking the dynode causes other electrons to be ejected from the dynode. This "multiples" the initial photocurrent, that is current pulse can be amplified and counted.

M.C.A/Computer- it has analogy-to-digital converter to arrange all the output pulses with respect to height. In addition, it has a software for proper spectral data acquisition and storage. The spectrum is displayed on the monitor, (Gao, 2003). Further illustration of the scintillation detector is shown in figure 3.11.

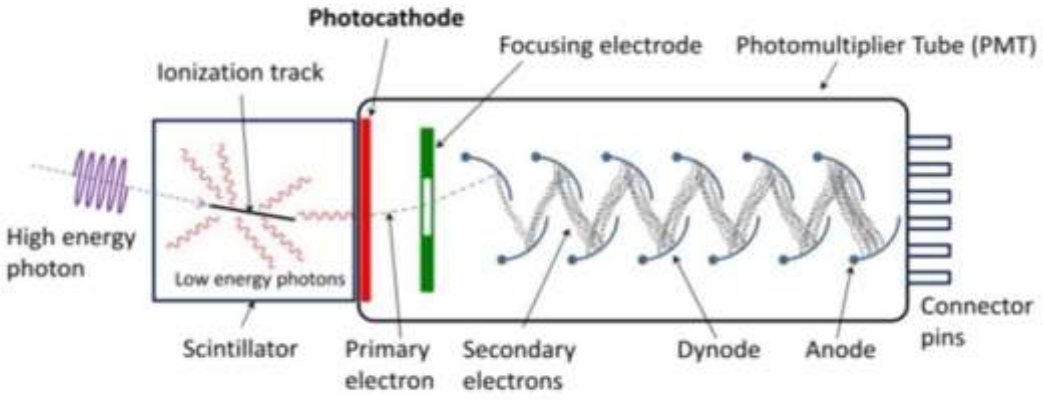

Figure 3.11: NaI(Ti) Scintillation detector (IAEA, 2004).

3.9 Counting Efficiency (n) of NaI(Ti)

This is a probability in which an emitted gamma ray would interact with the detector crystal and as a result cause a given count (Reguigui, 2006). The efficiency of any detector is pegged on three features namely; i) Detector size - efficiency of a detector increases with the increase of the size of the detector because a big detector provides a larger volume of gamma ray interaction and absorption, ii) Distance between the photon source and detector- the number of ionizing radiations detection efficiency is higher when the distance between the detector and the radiation source is at bare minimum and iii) Detector casing material thickness - A thin material at the entrance window will be preferred since it will minimize energy attenuation of incident gamma ray (Eberth & Simpson, 2008).

CHAPTER FOUR

MATERIALS AND METHODS

This chapter presents materials and devices used in the current research. Geology of the research site, sample assemblage, sample fashioning, and sample running are clearly discussed. Additionally, NaI(Ti) detectors energy calibration, energy resolution and counting efficiency are also presented. Lastly, a discussion on dosimetric parameters and hazard indices and their relevant formulae is done.

4.1 Materials and devices

Materials and devices used during data sampling, sample preparation and sample analysis are as follows; quarry samples stones from Kyasioni, Mavoloni and Kathaana quarries for radiometric analysis, Non-woven bags for holding the stone samples, Forty two 250 *ml* plastic containers for holding the samples, three large packaging boxes for holding the samples of the same quarry separate from the other quarries, Global Positioning System (GPS) enabled device (smart phone) to take the coordinates of the sampled points, aluminum foil for lining in the lids while corking the plastic containers to ensure no leakage of radioactive gases. Other requirements include labeling stickers for proper identification of the samples, oven for sample drying, digital weighing balance for exact weight measurement, gamma ray spectrometer system and a PC installed with Maestro software for spectrum acquisition relied upon during Multi-Channel Analyzer energy calibration, detector resolution and analysis. Additional materials and devices are Microsoft Excel and OriginPro for spectral data analysis, IAEA certified reference samples and multi-nuclide source (standard reference material).

4.2 Geology of the study area

This study was carried out in Kyasioni quarry, Mavoloni quarry and Kathaana quarry which are found in Machakos County. The County is bounded by the latitude:-1° 29' 59.99" S and longitude 37° 14' 66.00' E. This region is generally characterized by intensely folded basement systems of gneisses and schists, which have limestone, amphibolites, and quartzites. These rocks have both metamorphosed and granitized to a given extent, (Pulfrey, 1960) and therefore the dominant rocks in this county are both Metamorphic and

igneous. Metamorphic rocks are mainly formed from highly radioactive rocks and therefore they tend to be radioactive (Bucher & Frey, 2002). Granite rocks contain the highest primordial radionuclides, but the concentration of these radioactive elements decreases in igneous rocks (Hameed *et al.*, 2014).

Kyasioni quarry lies in the latitudes 0° 50' and 1° 30'S and the longitudes 37°30' and 37°55'E, Mavoloni quarry is within the latitudes 1°4'60''E and the longitudes 37°25'60''E while Kathaana quarry is in the region described by the co-ordinates 1°19'32''S and 37°17'19''E. Kyasioni quarry is found in Yatta plateau which is largely a level ground while Kathaana quarry sits in a little hilly area in Kangundo constituency. Some notable examples of rocks from these areas are kyanite, limestone, graphite schists and gneisses (Fairburn, 1963). The distance from Nairobi to Kyasioni quarry, Mavoloni Quarry (via Nairobi-Garissa Road), and Kathaana Quarry (via Kangundo road) are approximately 120.1 km, 84.5 km, and 77.0 km respectively. The proximity of the Kenyan capital (Nairobi) to these quarries, the quality of these rocks and their appealing appearance and the high demand for housing makes these quarry construction stones highly relied upon and hence the need for their radiological analysis to guarantee biological safety to the quarry workers and the house occupants. Figure 4.1 shows the relative geographical positions for Kyasioni, Mavoloni and Kathaana quarries within Machakos County.

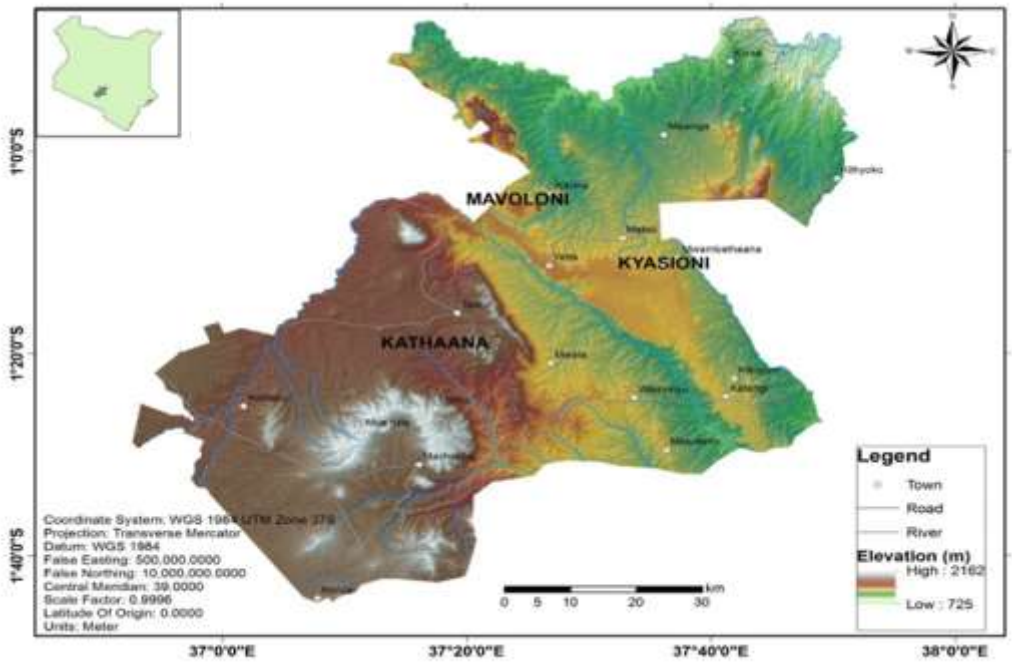

Figure 4.1: Relative positions of the three quarry sites**.**

4.3 Sample collection

Mining of construction stones from the three quarries under this study was found to be an exercise carried out in different but similar sub-sites. In each quarry sub-site, three to five individuals were directly involved in rock mining while another set of about two to three workers was arranging the cut-to-size rocks in rows and columns ready for transport to construction sites.

Random sampling technique was employed in the sample collection of forty-two quarry stone samples from the three quarry regions. Largely, the three quarry regions had almost the same quarrying character trends and therefore the same sampling method was adopted. This decision was also triggered by the fact that the three quarry sites are under similar geology. This sample size had an equal distribution from each quarry site to enhance proper comparison. The distance between sampling points was uneven due to the nature of the mining activities which was haphazardly done. For each specific point where a sample was collected, an enabled global positioning system device (mobile phone) was used to determine the co-ordinates as shown in Table 4.1. The co-ordinates were later used in coming up with sampling maps as shown in Figures 4.2, 4.3 and 4.4. Stone samples of approximate weight 270 grams were collected and independently placed in a non-woven (flexible) bag, labeled and kept in the holding box. The collected samples were about 270 grams because an exact measurement of 250 grams would be necessary for activity measurement. Samples from the three quarry sites were kept in three different labeled boxes.

Table 4.1: GPS co-ordinates from the sampled sites

Sample	Kyasioni quarry		Mavoloni quarry		Kathaana quarry	
	Latitude	Longitude	Latitude	Longitude	Latitude	Longitude
S1	S01º	E037º	S01º	E037º	S01º	E037º
	11.046’	36.186’	04.443’	24.182’	19.057’	17.472’
S2	S01º	E037º	S01º	E037º	S01º	E037º
	11.022’	36.179’	04.445’	24.171’	19.051’	17.473’
S3	S01º	E037º	S01º	E037º	S01º	E037º
	11.010’	36.190’	04.450’	24.173’	19.053’	17.461’
S4	S01º	E037º	S01º	E037º	S01º	E037º
	10995’	36.217’	04.458’	24.173’	19.047’	17.458’
S5	S01º	E037º	S01º	E037º	S01º	E037º
	10.979’	36.192’	04.465’	24.176’	19.030’	17.258’
S6	S01º	E037º	S01º	E037º	S01º	E037º
	10.959’	36.166’	04.473’	24.179’	19.016’	17.455’
S7	S01º	E037º	S01º	E037º	S01º	E037º
	10.948’	36.137’	04.479’	24.171’	19.005’	17.450’
S8	S01º	E037º	S01º	E037º	S01º	E037º
	10.889’	36.126’	04.489’	24.164’	19.003’	17.433’
S9	S01º	E037º	S01º	E037º	S01º	E037º
	10.824’	36.081’	04.495’	24.152’	19.001’	17.426’
S10	S01º	E037º	S01º	E037º	S01º	E037º
	11.319’	36.136’	04.492’	24.147’	18.993’	17.429’
S11	S01º	E037º	S01º	E037º	S01º	E037º
	11.369’	36.111’	04.188’	24.188’	18.950’	17.439’
S12	S01º	E037º	S01º	E037º	S01º	E037º
	11.406’	36.117’	04.456’	24.203’	18.944’	17.434’
S13	S01º	E037º	S01º	E037º	S01º	E037º
	11.361’	36.143’	04.432’	24.209’	18.941’	17.457’
S14	S01º	E037º	S01º	E037º	S01º	E037º
	11.389’	36.150’	04.423’	24.220’	18.950’	17.462’

Figures 4.2, 4.3 and 4.4 are as a result of the co-ordinates in Table 4.1.

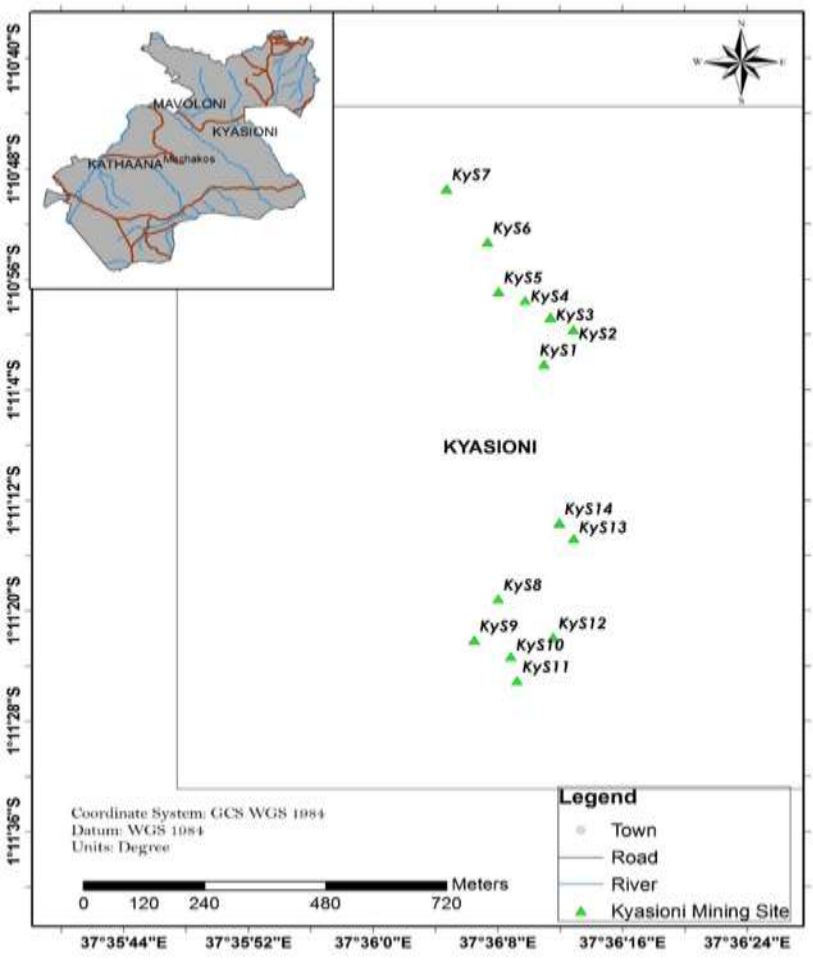

Figure 4.2: Kyasioni quarry site random sampling map

The cording KyS1 up to KyS14 indicates the exact positions were the individual rock sample was collected.

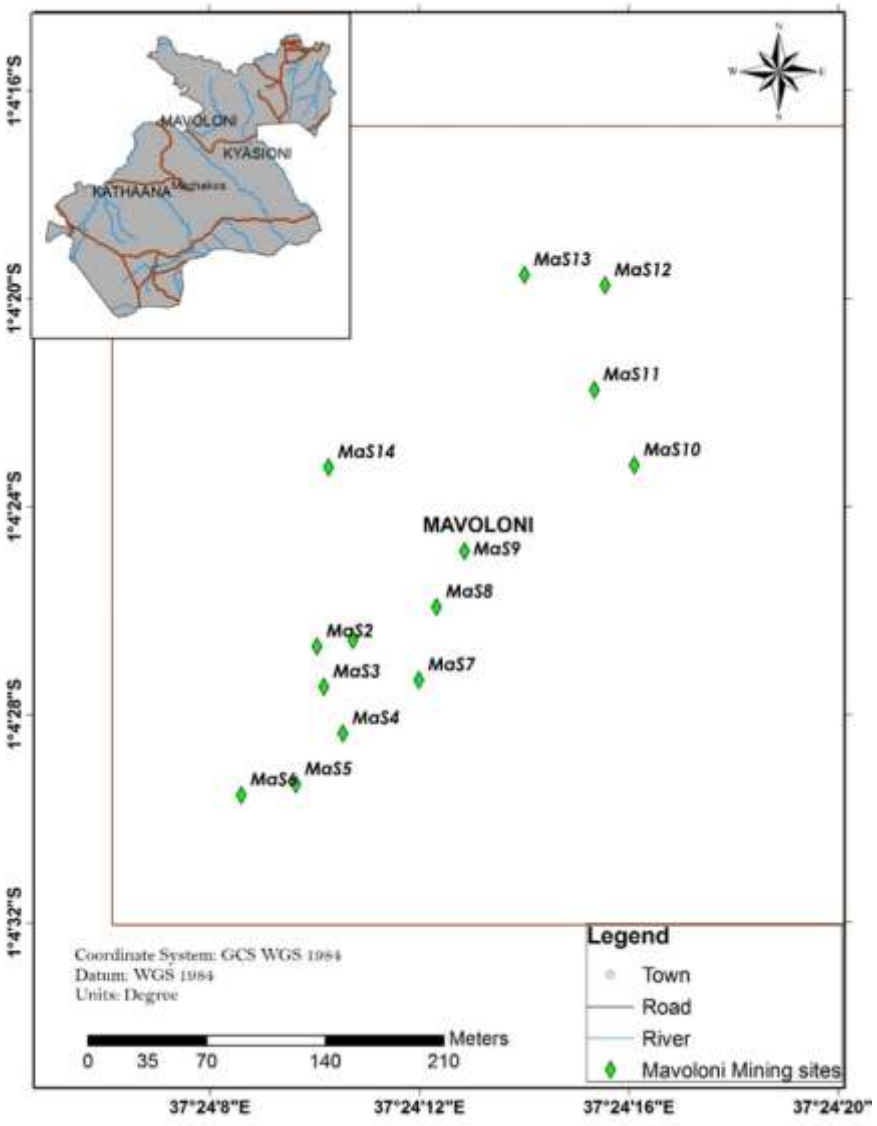

Figure 4.3: Mavoloni quarry site random sampling map

The labeling MaS1 up to MaS14 shows the sampling positions within Mavoloni quarry.

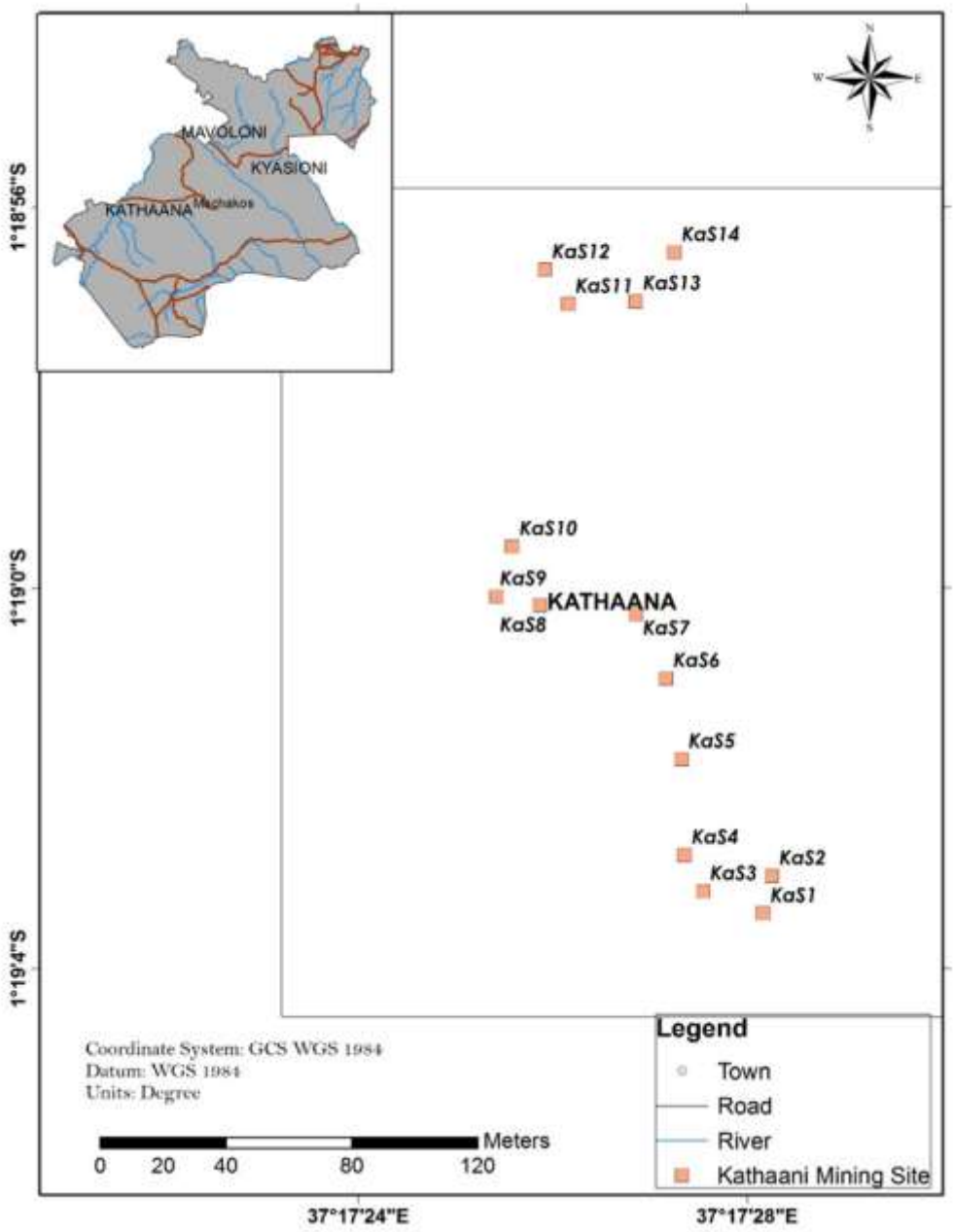

Figure 4.4: Kathaana quarry site random sampling map

The points KaS1 up to KaS14 shows how systematic random sampling was carried out in collecting samples within Kathaana quarry.

4.4 Sample preparation

The forty two collected rock samples were independently dried in an oven up to a temperature of 110º C since at this temperature the absorbed water by the rock samples was considered fully evaporated. This helped in attaining an even weight for all the samples and hence activity concentrations of ^{226}Ra, ^{232}Th and ^{40}K would be directly calculated (Benke & Kearfott, 999). The dry samples were later independently crushed and ground into fine powder for easy packaging as well as to increase the surface area for the detection of the perceived radionuclides. This exercise was done at Geology and Mines Laboratory in Nairobi.

Further, the sample rock powder was sieved through a 1 mm sieve for uniformity of the sample particles and repackaged into their respective non-woven bags. 250 grams of the sieved rock samples were independently measured and packaged into 250 *ml* plastic containers, and the lid, lined with aluminum foil replaced tightly. This was done to avoid leakage of ^{238}U and ^{232}Th and their daughter products of Radon and Thoron gases respectively. Under this state, the samples were stored for twenty-eight days for the radionuclides present and their daughter products to attain secular equilibrium (Papadopoulos *et al*., 2013).

4.5 Sample Running

NaI(Ti) detector of the model VG-BB-98/6D1, Drawing 10-01594, Order SO13397 2017, and of weight 1363 Kg found in the South Eastern Kenya University (SEKU) Physics laboratory was used for running the samples. Each sample was directly lodged on the detector's crystal since the container holding the sample had similar geometry as the detector. The measurement of each sample took 28800 seconds (real-time). After running all the geological samples, the emerging spectra were acquired and saved ready to recall for both qualitative and quantifiable analysis. The main procedure can be summarized as shown in Figure 4.5.

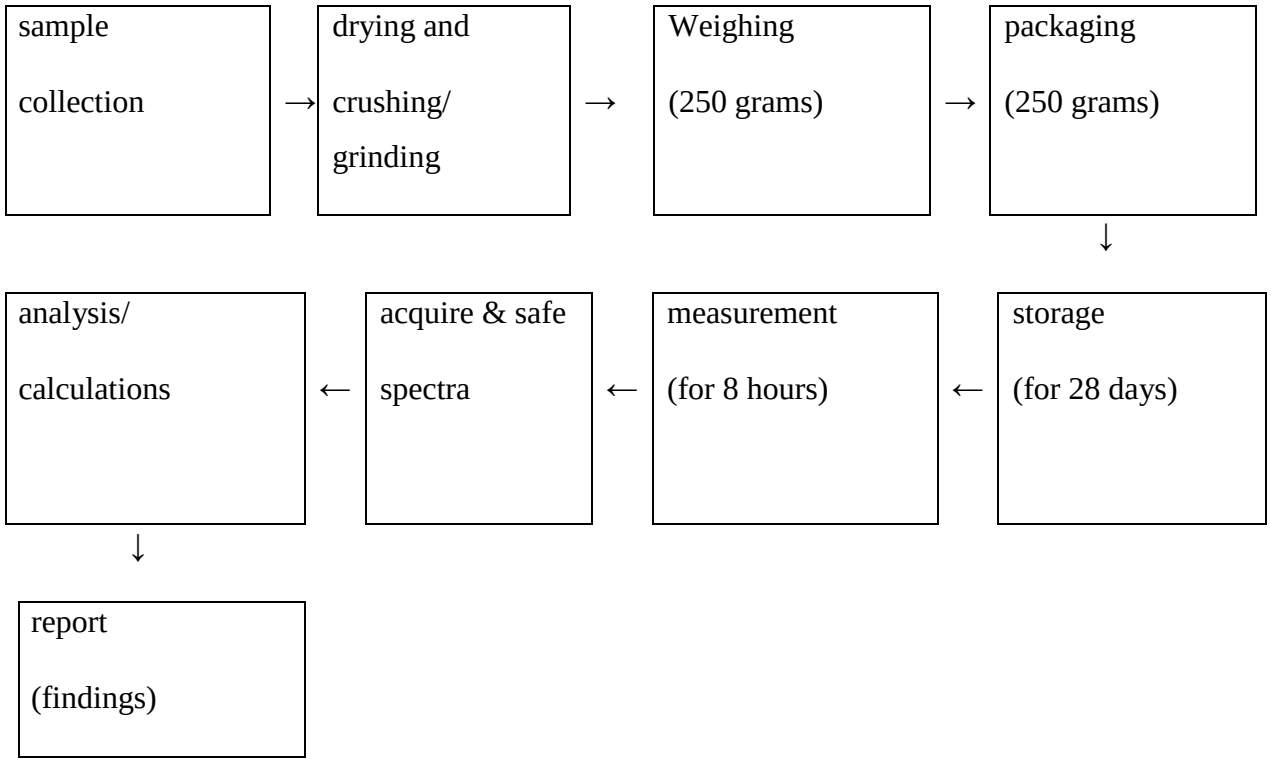

Figure 4.5: Block diagram of the procedure.

4.6 NaI(Ti) Detector

This study employed the use of NaI(Ti) gamma-ray spectrometer in the measurement of activity concentration of the samples. Before commencement of the actual counting, the MCA was calibrated and detector resolution and efficiency also done as discussed in the following subsections.

4.6.1 Energy calibration

The calibration of energy helps in aligning the detector's channel numbers with the energies of the detected gamma ray photons such that, one can correctly identify peaks representing certain radionuclides through the characteristic centroid energy (Gilmore, 2008). The connection between the channel and energy is given as a quadratic equation. Moreover, it is also necessary to repeat the energy calibration to eliminate channel-energy mismatch caused by variation of temperature since scintillation detectors are prone to effects of temperature transients (Goldsten *et al*., 2007).

Since the crystal functions under high voltage excitation, it may also be affected by mechanical vibrations. To avoid such impacts, the measurement system was neither

relocated nor disturbed. A standard reference material (SRM) (high activity concentration multi-nuclide sample) supplied by IAEA containing ^{137}Cs, ^{241}Am and ^{60}Co with characteristic gamma ray energies of 662 keV for ^{137}Cs, 59.5 Kev for ^{241}Am and both 1173 keV and 1332 keV for ^{60}Co was used for energy calibration (Scheinman, 2016). The corresponding channel energies are shown in Table 4.2.

Table 4.2: Energy calibration

Radionuclide	Energy (keV)	Channel
^{241}Am	60.0	34.1
^{137}Cs	663.35	329.6
^{60}Co	1172.69	565.5
^{60}Co	1332.69	637.3

Numerical data about the channels and energies obtained from the SRM spectrum's peaks was used for energy-channel fitting which is graphically presented in Figure 4.6.

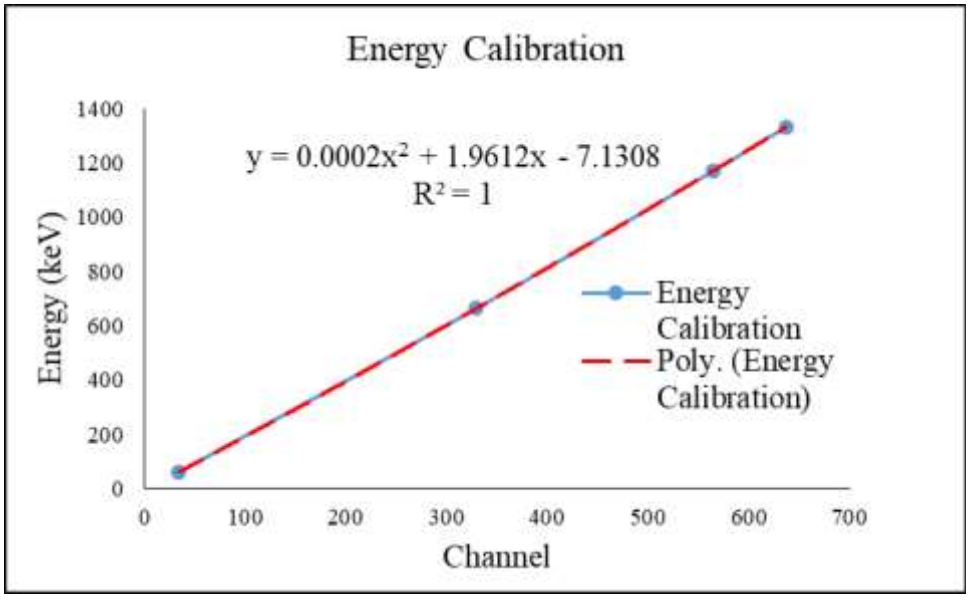

Figure 4.6: Energy calibration fit used in this study

The line in Figure 4.6 represents a second-order polynomial fit to the data generally defined in form of equation 4.1

$$y(x) = kx^2 + nx + m \qquad 4.1$$

Where y is the resultant photon energy, x is the channel number and k, n and m are the fit constants (Shikali, 2013). The values for the fit constants k, n and m from the SRM are clearly visible from the polynomial shown by equation 4.2.

$$y = 0.0002x^2 + 1.9612x - 7.1308 \qquad 4.2$$

Where $k = 0.0002$, $n = 1.9612$ and $m = -7.1308$ $(the\ y - intercept)$.

The fitting of these energy points is very significant since it helps in identification of the energies of unspecified photon peaks within the spectrum that is relied upon during nonquantitative examination.

Due to the long period of time of observations, (28800 seconds) the poison distribution observed in nuclear events for a short time normally assumes a Gaussian distribution (Bohm, & Zech, 2014). Thus, a Gaussian curve was used to fit the photo peak and validate the theoretical stipulation. Equations 4.3 and 4.4 show the poison and Gaussian distributions respectively. N represents the number of observations.

$$\boldsymbol{P_N = \frac{N^{-N} e^{\overline{-N}}}{N!}} \qquad \mathbf{4.3}$$

$$\boldsymbol{y = \sum_{i=1}^{n} a_i e \left[-\left(\frac{x - b_i}{c_i^2} \right)^2 \right]} \qquad \mathbf{4.4}$$

In equation 4.4, a, b, c and n are the amplitude, centroid location, width of the peak and number of the peaks respectively.

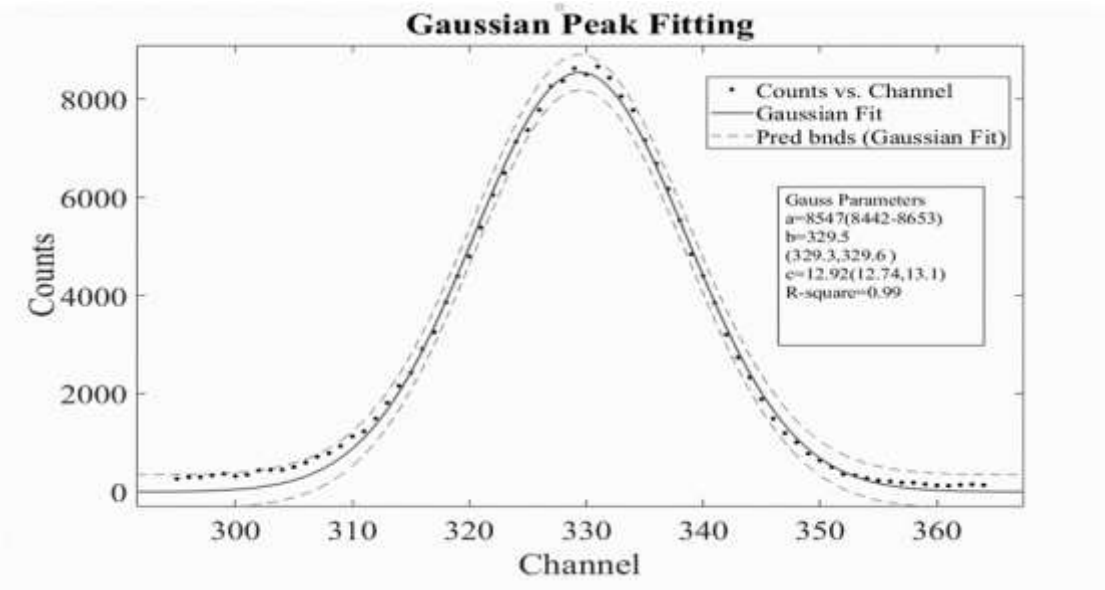

Figure 4.7: Gaussian fitting for ^{137}Cs Photo-peak at 663.35 KeV

As seen in Figure 4.7, the centroid location for the fitted curve is channel 329.5 while for the raw data is 329.6. The Gaussian fitting is very precise for fitting nuclear events observed over a long duration leading to many events. On the other hand, the R-square value is 0.99 which is close to 1 implying an excellent fit. The prediction boundary lines are also close to the raw data plot an indication of Gauss preciseness in fitting a gamma photo peak.

4.6.2 Energy Resolution

Energy Resolution is the measure of the width of a single energy peak at a specific energy. Better resolution (lower FWHM value) leads to clear peak separation within spectrum. At an energy of 662 keV, NaI(Ti) gives a resolution of about 7% (Wang, 2003). NaI(Ti) detector has a slow response and hence they are not ideal for applications involving high-count rates. Also, their poor resolution results in broad peaks that overlap hence making spectroscope applications involving multiple isotopes considerably more challenging. In this work, the energy resolution was determined at three energies as shown in Table 4.3. The resolution was obtained from equation 4.5 which shows that full width at half maximum (FWHM) is fundamental in determination of the resolution at each energy.

$$R = \frac{FWHM}{E_C} \quad 4.5$$

Where $E_c$is the photo peak energy given by the centroid of the signal.

Table 4.3: Energy resolution

Radionuclide	Energy (keV)	FWHM	Resolution
^{137}Cs	663.35	43.78	6.6%
^{60}Co	1172.69	55.59	4.7%
^{60}Co	1332.69	60.09	4.5%

Figure 4.8 gives a graphical presentation of resolution as determined in Table 4.3 against the radionuclides' centroid energy.

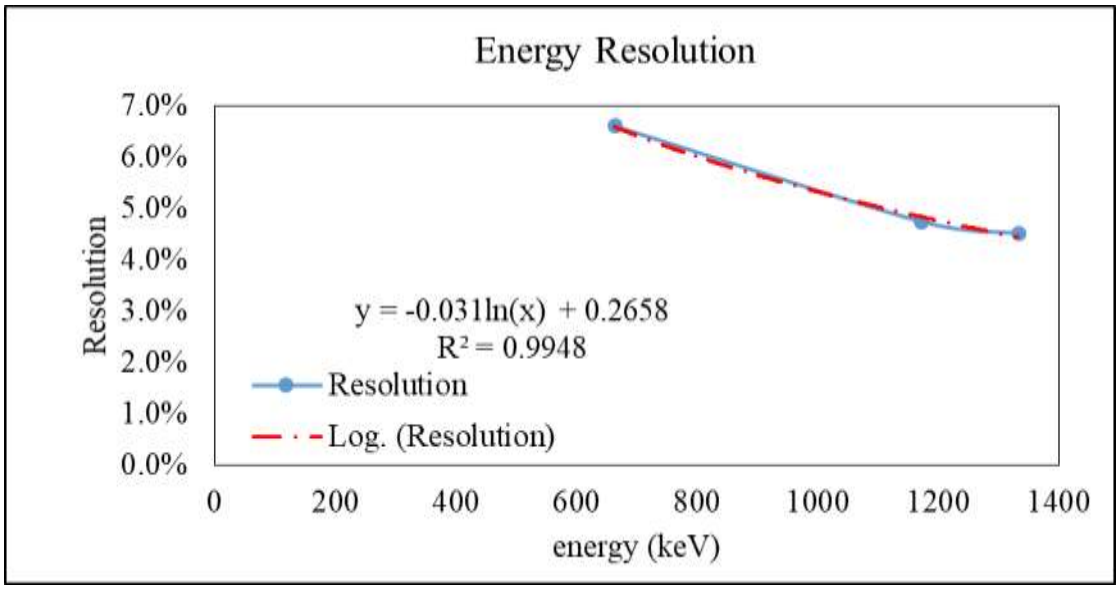

Figure 4.8: Energy resolution

Clearly, from Figure 4.8, the energy resolution was observed to decrease with increase in the photo peak energy. A logarithmic fitting resulted to an R-square value of 0.99 that revealed a close to perfect fit. The relationship between energy resolution and photo peak is in form of a general equation 4.6.

$$y(x) = Aln(x) + B \quad 4.6$$

Where y is the resolution, x is the photo peak energy and A and B are fit parameters. The values of A and B are gotten from equation 4.7 as 0.031 and 0.2658 respectively.

$$y(x) = -0.031ln(x) + 0.2658 \quad 4.7$$

When second order polynomial was used, it resulted to an R-square value of 1 which was deemed as curve over fitting thus rejected. The trend of energy resolution and energy shown imply that higher energy peaks are broader while the lower ones are much resolved hence narrow. This can be observed by the increasing FWHM with energy.

4.6.3 Counting Efficiency

Counting efficiency is defined as the probability that a discharged gamma ray will interact with the detector crystal and cause a given count (Reguigui, 2006). NaI(Ti) detector functions by scintillation mechanism. Unlike semiconductor gamma ray detectors, NaI(Ti) detector does not suffer long dead times. Since the gamma source was placed on the detector, the distance between the sample and the detector was 0 cm which meant that with the 0.01% dead time of the detector, the detection efficiency was very high. This was verified by comparing the live time and dead times of the detector at the end of each counting run. Therefore, the gamma detector used greatly reduced the chances of missing an emitted photon. From this work, the efficiency for the standard radionuclides were determined from equation 4.8.

$$\eta = \frac{N}{AM\rho T} \quad 4.8$$

Where N is the net count rate, T is the live time, ρ is the radionuclide's emission probability, M is mass in kilograms for the standard sample and A the activity concentration of the standard sample.

Table 4.4: Detectors' efficiency and intensity for the standard radionuclides used in this work

Nuclide	Energy (KeV)	Intensity	Emission probability	Activity	Mass (Kg)	Efficiency (η)
^{232}Th	238	26.46661	0.4316	3250	0.236	0.079951
^{238}U	351	19.5907	0.3534	4940	0.239	0.046952
^{40}K	1460	8.757	0.1066	14000	0.279	0.021031

4.6.4 Measurement of the background radiation

The gross count registered by the detector when geological samples were measured was inclusive of background count from natural or artificial sources within the detector. Examples of natural sources include cosmic radiation and terrestrial gamma radiation. The exact net count of the geological spectra samples was determined by subtracting the background spectrum acquired after running deionized water from each geological sample spectrum. This was key for quality and reliable radiometric survey data in this research work. To obtain the background spectrum, deionized water was run for 28800 seconds under the exact conditions as the geological samples.

Water has high concentration of ions mainly from the soil. Examples of these ions are sodium, calcium, iron, copper sulfates, carbonates, and nitrates (Alam *et al*., 2012). Water devoid of these ions is said to be deionized. Deionized water was used for background counting because it does not contain radionuclide particles and therefore any counts registered during its' running are said to be from the detector's surrounding environment. Figure 4.9 shows a geological spectrum from sample KyS1 that was acquired after a live time of 28793 seconds. The real time was set as 28800 seconds.

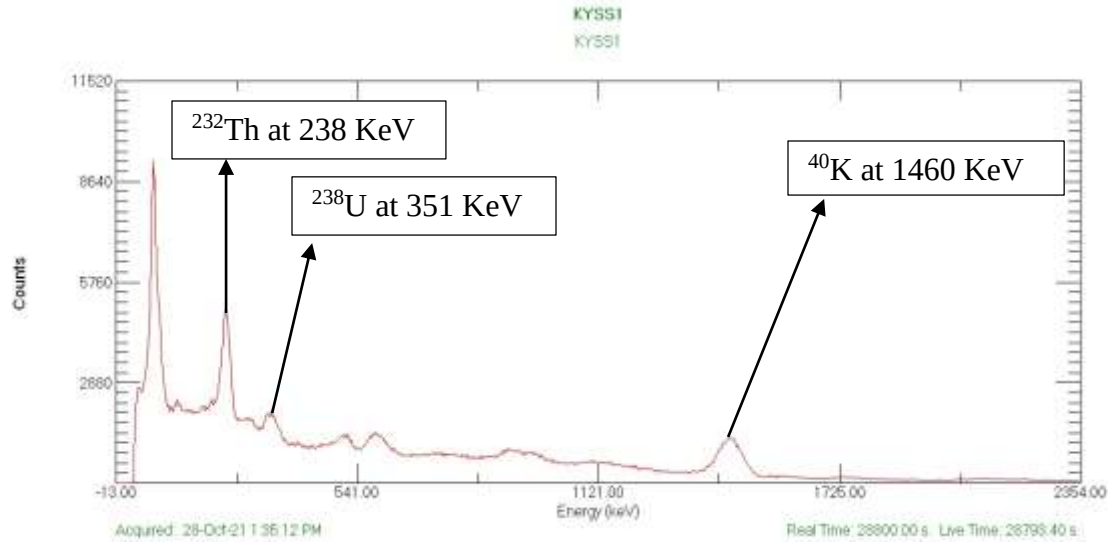

Figure 4.9: Kyasioni quarry sample KyS1 spectrum

4.7 Activity concentration (Bq/Kg)

The activity of the prepared sample stones from each quarry was measured separately. Radionuclides from ^{238}U and ^{232}Th series were ascertained from gamma peaks of their short-lived decay products. These decay products are ^{214}Bi and ^{214}Pb at energies of 609 KeV and 351 KeV respectively for ^{238}U while ^{228}Ac at 911 KeV and ^{212}Pb at 238 KeV resembles ^{232}Th. ^{40}K gives a single photo-peak at an energy of 1460 keV and therefore it was identified from this peak.

The radiation activity concentration for the three radionuclides of interest was calculated from equation 4.9 (Ebaid, 2010).

$$A_c = \frac{I}{\rho . n . m} (Bq/Kg) \qquad (4.9)$$

Where I is the intensity, ρ is the emission probability for gamma ray, n is the photo peak efficiency of the detector system, and m is the mass of the measured stone sample in kilogram.

The intensity I was calculated from the equation 4.10.

$$I = \frac{N}{T} \qquad 4.10$$

Where *N* is the net count and *T* the live time.

4.8 Radium Equivalent Activity (Ra_{eq})

This is the weighed sum of activities of the primordial radionuclides. The determination for the numerical value of Ra_{eq} is founded on the assumption that 370 Bq/kg of ^{226}Ra, 259 Bq/kg of ^{232}Th and 4810 Bq/kg of ^{40}k yield equivalent gamma radiation dose rate (Ahad, *et al*., 2004).

Its' calculation was done from equation 4.11

$$Ra_{eq} = A_{Ra} + \frac{10}{7}A_{Th} + \frac{10}{130}A_K \qquad 4.11$$

where, A_{Ra}, A_{Th} and A_k are the activity concentration of ^{226}Ra, ^{232}Th and ^{40}k respectively. $\frac{10}{7}$ is the conversion factor for thorium while $\frac{10}{130}$ is conversion factor for potassium.

4.9 Total Absorbed Dose Rate in Air (D)

Our immediate environment absorbs radiations emitted by primordial radionuclides. To calculate this absorbed dose rate, the conversion factors as provided by UNSCEAR, 2017 are needed. The conversion factors for activity concentration of ^{226}Ra, ^{232}Th and ^{40}k into dose are given as 0.427, 0.662 and 0.043 respectively. Equation 4.12 was employed in the determination of total effective dose rate in air.

$$D = (0.427C_{Ra} + 0.662C_{Th} + 0.43C_K)\ nGy/h \qquad 4.12$$

Where C_{Ra}, C_{Th} and C_K are the specific activity concentration for ^{226}Ra, ^{232}Th and ^{40}k in the sampled quarry stones respectively.

4.10 Annual Effective Dose Rate (AEDR)

This is the individual's total radiation risk when inside (indoor) or outside (outdoor) buildings. It's assumed that on average, a Kenyan adult spend 40% of his/her time outdoor and 60% indoor, (Mustapha *et al*., 1999). The worldwide mean outdoor and indoor occupancy factors are given as 20% and 80% respectively (UNSCEAR, 2010). The annual effective dose (AEDR) was calculated from equation 4.13.

$$AEDR = D \times T \times C \times 10^{-6} \qquad 4.13$$

Where D is the absorbed dose, T is the occupant time and C is the dose conversion factor (converts the absorbed dose in the air to human effective dose).

The calculation of the AEDR in Kenya, when indoors (E_{in}) and when outdoors (E_{out}) was done with respect to the conversion factors of 60 % (0.6) and 40% (0.4) respectively. The equations used were 4.14 and 4.15 respectively.

$$E_{in} = D(nGy/h) \times 8760\ (h/y) \times 0.6 \times 0.7(Sv/Gy)10^{-6} \qquad 4.14$$

$$E_{out} = D(nGy/h) \times 8760\ (h/y) \times 0.4 \times 0.7(Sv/Gy) \times 10^{-6} \qquad 4.15$$

Where, D is the absorbed dose, 8760 h/y is the time in hours for one year, 0.7 (Sv/Gy) is the dose conversion factor and 0.6 and 0.4 are the indoor and outdoor occupancy factor respectively (Mustapha *et al*., 1999).

4.11 External Radiation Hazard Index (H_{ex})

This is the degree of outermost exposure to overabundance gamma radiation mainly from primordial radionuclides emitted by construction materials. The outermost body exposure to too much gamma radiation from these radionuclides is hazardous.

The maximum value allowed for H_{ex} is a unity and it matches the highest radium equivalent activity of 370 Bq/kg (Al-Zahrani, 2017). Equation 4.16 was used to calculate H_{ex} (Beretka & Mathew, 1985)

$$H_{ex} = \frac{A_{Ra}}{370} + \frac{A_{Th}}{259} + \frac{A_K}{4810} \qquad 4.16$$

Where A_{Ra}, A_{Th} and A_k are activity concentration of radium, thorium and potassium respectively.

4.12 Internal hazard index (H_{in})

Internal hazard index is mainly the internal exposure arising from radon gas and its short-lived decay products. This occurs on inhalation of terrestrial radionuclides from ^{238}U, ^{232}Th and ^{40}k decay series radionuclides (Tsai *et al*., 2008). Internal hazard index was estimated by use of equation 4.17 (Beretka & Mathew, 1985).

$$H_{in} = \frac{C_{Ra}}{185} + \frac{C_{Th}}{259} + \frac{C_K}{4810} \qquad 4.17$$

Where C_{Ra}, C_{Th} and C_K are the mean activity concentration for ^{226}Ra, ^{232}Th and ^{40}k in Bq/kg respectively.

CHAPTER FIVE

RESULTS AND DISCUSSIONS

5.1 Introduction

This chapter contains findings of the research regarding radiological information of stone samples from the three quarry sites namely Kyasioni, Kathaana and Mavoloni using gamma -ray spectroscopy analysis. Accompanying Figures and Tables hold the data about the radiological parameters of the samples in the respective quarries. The activity concentration of the samples from each quarry is presented and discussed. A comparison of activities among the three quarries is also performed. The average activity from each quarry was used to compute all other radiological parameters to avoid duplicating calculations and data presentations. Thus, radiological parameters reported in each quarry are an average value computed from 14 samples from each quarry. Further, a comparison of the results from the three quarries has been done.

5.2 Activity Concentration

The specific activity concentrations of ^{40}K for the 42 stone samples from the three quarries were determined and tabulated as shown in Table 5.1. In Figure 5.1, the activity concentration of ^{40}K for the forty-two geological representatives have been presented. The maximum concentration of ^{40}K was 1261.33 ± 32.27 Bq/kg from sample KyS4 of Kyasioni quarry while the least was 841.16 ± 29.91 Bq/kg from Mavoloni quarry sample MaS3. In addition, the mean activity concentration was 1120.35 ± 30.07 Bq/Kg, 1019.17 ± 29.79 Bq/Kg and 1112.55 ± 30.97 Bq/Kg for Kyasioni, Mavoloni and Kathaana quarries respectively.

^{232}Th activity concentration data values determined from all the geological samples is presented in Table 5.2. A subsequent graphical comparison is presented in Figure 5.2. The maximum outcome for ^{232}Th activity concentration was 136.05 ± 2.55 Bq/Kg from sample KyS9 of Kyasioni quarry while the least was 65.21 ± 1.45 Bq/Kg for sample KaS3 from Kathaana quarry. The mean specific activity concentration for ^{232}Th was 118.48 ± 1.91 Bq/Kg, 105.52 ± 1.97 Bq/Kg and 81.82 ± 1.62 Bq/Kg from Kyasioni, Mavoloni and Kathaana quarries respectively. A similar presentation for ^{238}U activity concentration data

values for the three quarries is shown in Table 5.3 whose accompanying comparison graph is given as Figure 5.3. Kyasioni's sample KyS4 had the maximum ^{238}U activity concentration of 116.33 ± 3.89 Bq/Kg while the least computed value of 47.55 ± 2.86 Bq/Kg was from sample MaS4 of Mavoloni quarry. The average ^{238}U activity concentration from Kyasioni, Mavoloni and kathaana quarries was 74.75 ± 3.15 Bq/Kg, 67.00 ± 3.09 Bq/Kg and 63.25 ± 3.08 Bq/Kg respectively.

The determined activity concentration values for the primordial radionuclides namely ^{40}K, ^{232}Th, and ^{238}U from all the forty-two geological samples exceeded the permissible limits of 420 Bq/Kg, 45 Bq/Kg and 33 Bq/Kg respectively (UNSCEAR, 2010). Additionally, the ^{40}K activity concentration was higher than that of both ^{232}Th, and ^{238}U. This elevated ^{40}K concentration level was attributed to its dominance in the Earth's crust. The higher activity concentration of ^{232}Th, and ^{238}U was contributed by weathering of granite rocks during quarrying activities (Alnour *et al*., 2012). Further, the heavy vehicles accessing the quarry sites to transport these rocks enhance the weathering of the rock cuttings along the quarry access roads since they exert high pressure on them hence breaking them into tiny pieces. Moreover, the exposure of rocks such as monazites, igneous, and quartzites (during quarrying activities) is also a major source of the elevated activity levels (Shikali, 2013).

It should be noted that, for simplicity purposes of plotting and comparison of the samples from the three quarries, the sample naming was altered such that S1 represents sample KyS1, KaS1 and MaS1 while S2 represents samples KyS2, KaS2 and MaS2 and so on up to S14 which represented samples KyS14, KaS14 and MaS14. Likewise the color coding represents the three quarry sites and the concentration limits.

Table 5.1: ^{40}K Activity concentration

	^{40}K Activity Concentration (Bq/Kg) for the three quarries					
Sample	Kyasioni	Error	Mavoloni	Error	Kathaana	Error
S1	1121.70	±29.70	1221.67	±31.53	1058.25	±31.61
S2	1207.21	±31.96	1174.13	±30.97	1116.32	±29.75
S3	1079.31	±29.35	841.16	±29.91	1102.26	±31.62
S4	1261.33	±32.27	850.35	±30.28	1051.91	±28.75
S5	1016.88	±29.35	864.75	±29.04	1196.87	±30.75
S6	1079.50	±30.28	1045.70	±28.79	1179.31	±34.47
S7	1236.07	±29.73	977.13	±28.11	1175.15	±31.31
S8	1046.54	±29.17	1186.79	±30.53	1112.68	±34.28
S9	1134.39	±29.29	1097.68	±28.79	1136.61	±30.19
S10	918.49	±28.86	901.63	±28.37	1141.95	±31.31
S11	1084.09	±30.47	947.19	±30.67	1010.02	±27.57
S12	1219.73	±30.72	1088.02	±30.66	1157.59	±31.75
S13	1139.84	±30.24	1049.73	±31.21	1124.45	±30.31
S14	1139.86	±29.66	1022.43	±28.24	1012.38	±29.87
Average	**1120.35**	**±30.07**	**1019.17**	**±29.79**	**1112.55**	**±30.97**

The values in Table 5.1 were used in coming up with the bar graph in Figure 5.1 which compares the specific activity concentration of ^{40}K from three quarries.

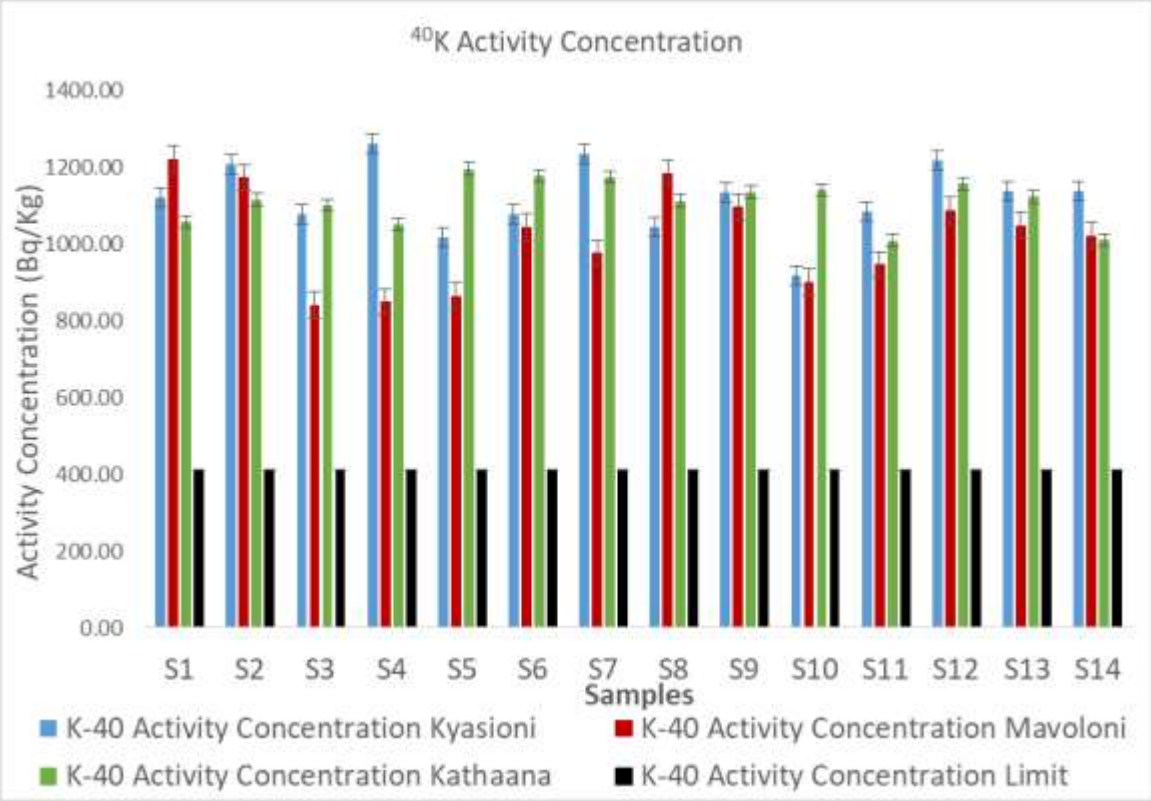

Figure 5.1: Activity concentration of ^{40}K from the three quarries

Table 5.2 presents the specific activity for ^{232}Th as determined from the three quarries.

Table 5.2: ^{232}Th Activity concentration

	^{232}Th Activity Concentration (Bq/Kg) for the three quarries					
Sample	Kyasioni	Error	Mavoloni	Error	Kathaana	Error
S1	108.30	±1.73	101.83	±1.75	80.93	±1.55
S2	120.48	±1.75	109.04	±2.31	81.00	±1.53
S3	112.04	±2.01	115.51	±2.18	65.21	±1.45
S4	120.37	±1.76	121.03	±2.52	84.00	±1.74
S5	117.71	±1.77	108.17	±1.85	88.76	±1.72
S5	127.25	±1.87	103.71	±2.15	81.71	±1.86
S7	100.06	±1.60	110.79	±2.25	75.02	±1.46
S8	104.65	±1.65	117.66	±1.96	81.38	±1.69
S9	136.05	±2.55	103.66	±1.76	85.88	±1.56
S10	131.00	±2.70	88.93	±1.86	85.88	±1.61
S11	125.88	±1.83	97.61	±1.86	85.88	±1.48
S12	130.02	±1.96	114.79	±1.97	82.50	±1.76
S13	116.85	±1.96	88.82	±1.52	82.90	±1.66
S14	108.07	±1.66	95.78	±1.64	84.43	±1.65
Average	**118.48**	**±1.91**	**105.52**	**±1.97**	**81.82**	**±1.62**

Graphical presentation of the data in Table 5.2 has been done in Figure 5.2.

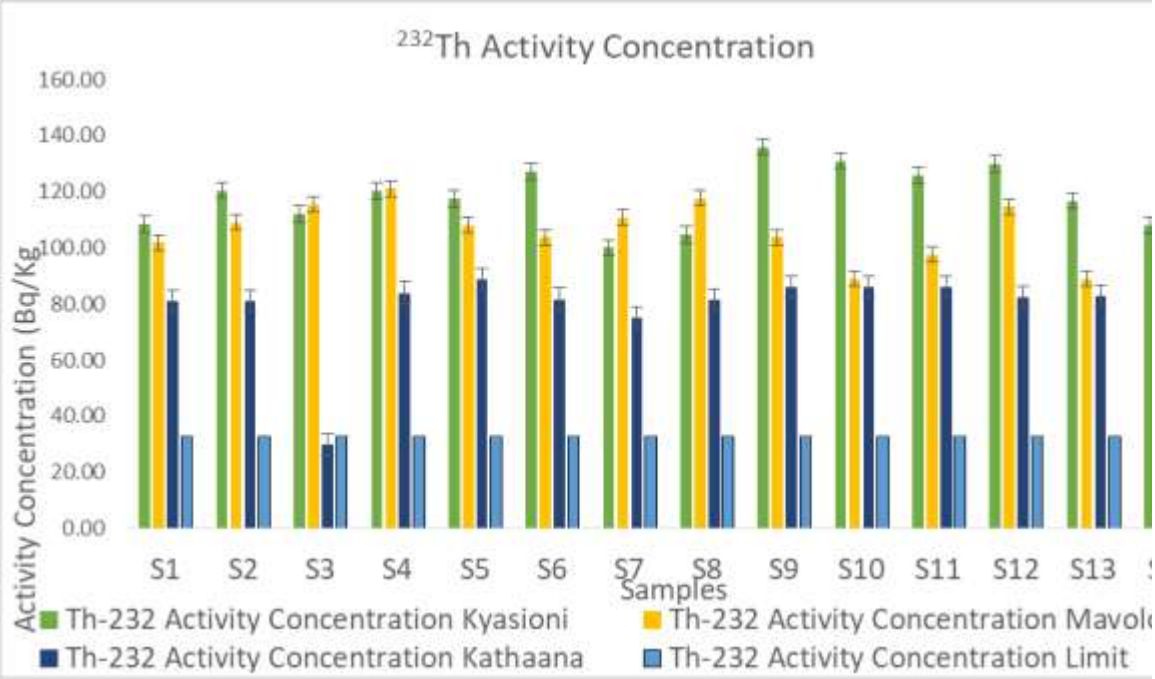

Figure 5.2: Activity concentration of ^{232}Th from the three quarries

Table 5.3: ^{238}U Activity concentration

	^{232}U Activity Concentration (Bq/Kg) for the three quarries					
Sample	Kyasioni	Error	Mavoloni	Error	Kathaana	Error
S1	56.07	±2.88	66.88	±2.85	69.87	±3.66
S2	77.74	±3.34	80.15	±3.15	66.69	±2.95
S3	53.08	±2.56	59.37	±2.88	55.46	±2.94
S4	116.33	±3.89	47.55	±2.86	69.95	±3.32
S5	69.56	±3.00	63.76	±3.04	65.40	±3.20
S6	92.28	±3.38	64.38	±2.94	68.30	±3.31
S7	59.50	±3.07	81.87	±3.29	64.84	±2.94
S8	73.64	±3.00	64.98	±3.01	58.51	±3.39
S9	54.28	±3.04	50.07	±2.84	60.96	±2.90
S10	63.05	±3.18	74.98	±3.20	74.48	±3.20
S11	102.34	±3.36	82.92	±3.47	53.48	±3.13
S12	107.39	±3.48	60.65	±3.27	52.27	±3.00
S13	77.24	±3.28	72.29	±3.39	74.66	±3.45
S14	43.95	±2.59	68.19	±3.13	50.64	±1.68
Average	**74.75**	**±3.15**	**67.00**	**±3.09**	**63.25**	**±3.08**

^{232}U activity concentration results from Table 5.3 is graphically analyzed in Figure 5.3.

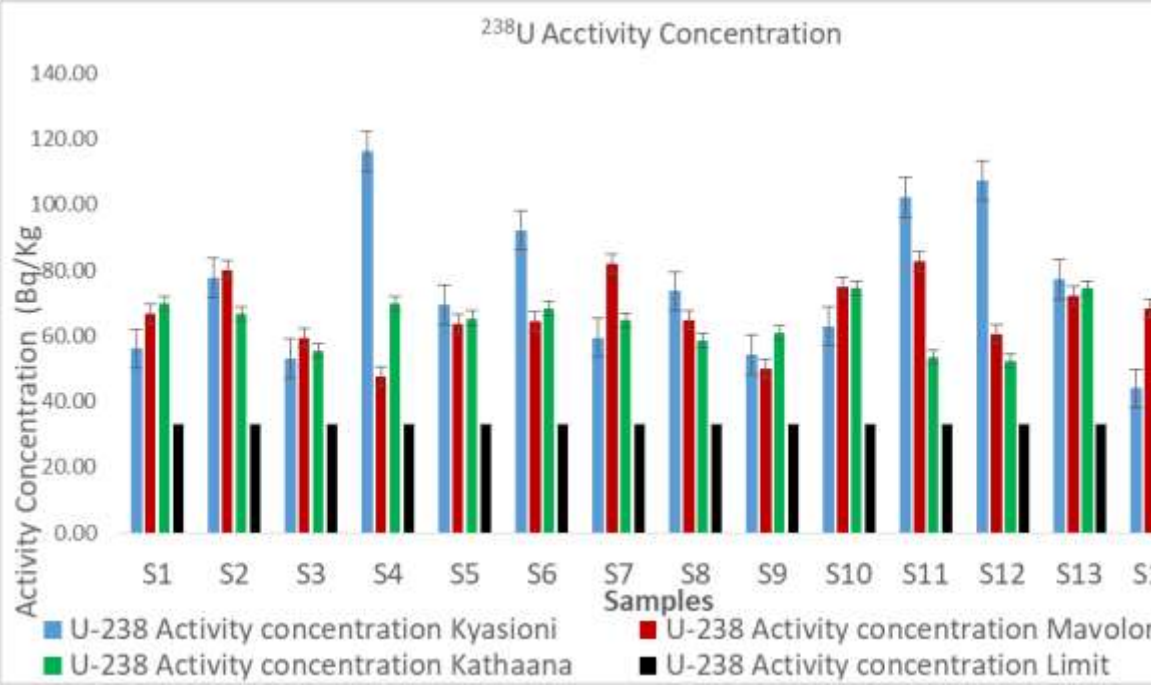

Figure 5.3: Activity concentration of ^{238}U from the three quarries

The activity concentration variation was noted across the 42 samples (14 samples from each quarry) from the three quarries which agrees well with the literature (Tzortzis *et al*., 2004, UNSCEAR, 2017) This variation in activity concentration is as result of geological constituents and chemical speciation of the individual geological sample. The activity concentration of the 14 representatives from every individual quarry averaged 74.75 ± 3.15, 67 .00 ± 3.09 and 63.25 ± 3.08 Bq/kg for ^{226}Ra, 118.48 ± 1.91, 105.52 ± 1.97and 79.30 ± 1.62 Bq/kg for ^{232}Th and 1120.35 ± 30.07, 1019.17 ± 29.79 and 1112.55 ± 30.97 Bq/kg for ^{40}K for Kyasioni, Mavoloni and Kathaana quarries respectively as presented in Table 5.4. The average activity concentrations of ^{226}Ra, ^{232}Th and ^{40}K was more than twice the world's mean figures of 33, 45 and 420 Bq/kg respectively (UNSCEAR, 2017).

Table 5.4: Average activity concentration

Quarry	Activity concentration (Bq/kg)		
	^{226}Ra	^{232}Th	^{40}K
Kyasioni	74.75 ± 3.15	118.48 ± 1.91	1120.35 ± 30.07
Mavoloni	67 .00 ± 3.09	105.52 ± 1.97	1019.17 ± 29.79
Kathaana	63.25 ± 3.08	79.30 ± 1.62	1112.55 ± 30.97
Average	**68.33 ± 3.11**	**101.10 ± 1.83**	**1084.02 ± 30.28**

The radioactivity trend reported by this work was in agreement with the world's trends of ^{40}K>^{232}Th>^{226}Ra (UNSCEAR, 2010). The moderate variations in the specific mean activity concentrations of ^{226}Ra, ^{238}U and ^{40}K among the quarries were inferred to the similarity in geological profile as the region is dominated by metamorphic substratum. Besides geology, variation in quarry depths may have influenced the concentrations of activity as the sampled quarries have different depths, an observation which has been made in similar studies (Bala, 2022).

5.3 Dosimetric Parameter Analysis

Calculation of the dosimetric parameters was independently done from the average concentration values obtained in each quarry. The computations were done by substituting the relevant variables and constants in the respective equations as discussed in chapter four. The results were compared among the quarries and graphical presentations done.

5.3.1 Total Absorbed Dose Rate in Air ($\boldsymbol{D}$)

The determined specific activity concentration of the three radionuclides from quarries studied were transformed to absorbed dose (D) in the air through the procedure and data provided by other investigators as presented in chapter four. A graphical comparison of the findings for the three quarries is presented in Figure 5.4

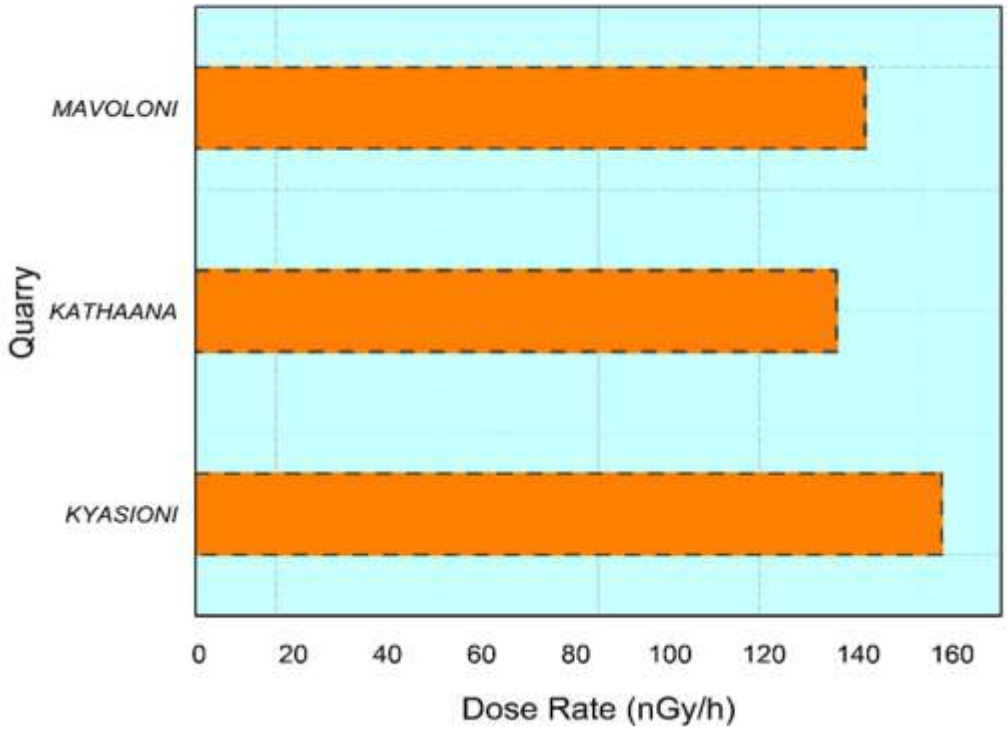

Figure 5.4: Comparison of Absorbed Dose Rate among the quarries

Due to variation in specific activity concentration, the average absorbed dose ranged from 128.95 ± 3.72 nGy/hr (Kathaana) to 158.45 ± 3.90 nGy/hr (Kyasioni) with an overall mean of 143.21 ± 3.81 nGy/hr. The overall dose mean was beyond 60 nGy/hr which is the world's average by about 2.38 times (Harb *et al*., 2012). The higher values for the absorbed dose rates were attributed to the elevated levels of ^{40}K activity concentrations from the samples studied.

5.3.2 Radium Equivalent Activity (Ra_{eq})

The average Ra_{eq} for all examined samples from the three quarries was within the radiological safe limit of 370 Bq/Kg (UNSCEAR, 2017) as shown in Figure 5.5. Referring to Table 5.4, the highest and lowest Ra_{eq} were 329.61 ± 8.18 Bq/kg and 265.35 ± 7.77 Bq/kg for Kyasioni and Kathaana quarries respectively. Mavoloni quarry had a value of 295.64 ± 8.19 Bq/Kg. These average values from the three quarries implies that construction materials from the three quarry sites under this study had no significant harmful radiological effect as far as the weight sum of the three radionuclides is concerned.

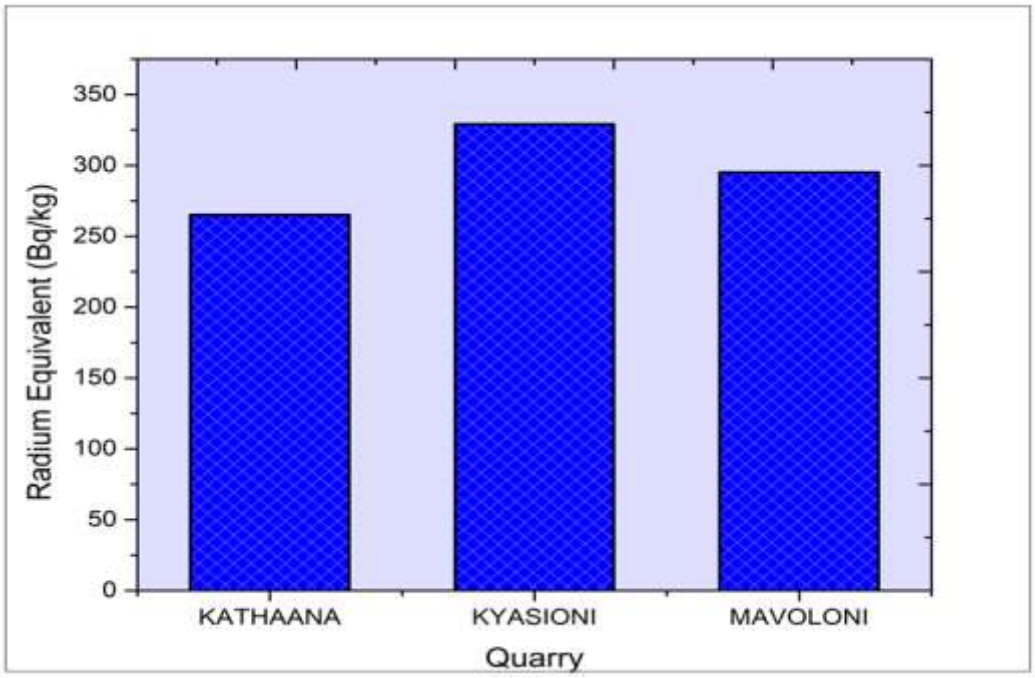

Figure 5.5: Radium equivalent activity comparison among the quarries.

5.3.3 Annual Effective Dose Rate (AEDR)

The annual effective dose rate is computed from the hourly absorbed dose rate in air to capture the effect of this dose on human body over a period of one year. Figure 5.6.gives a graphical comparison for the average AEDR among the quarries.

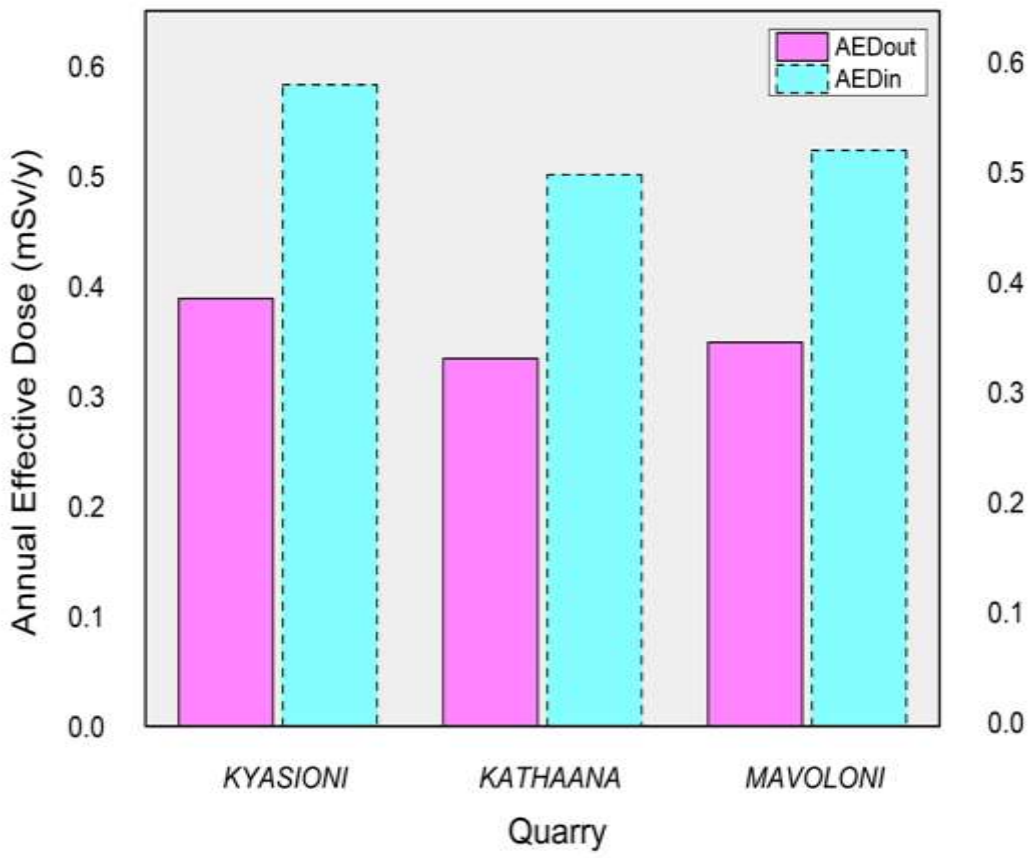

Figure 5.6: A comparison of annual effective dose rate among the quarries

The annual effective dose rate is broken into indoor and outdoor where the permissible AEDR is 1.2 mSv/y (UNSCEAR, 2010) for building materials. Rock samples from Kyasioni quarry contributed the highest indoor AEDR of 0.58 ± 0.01 mSv/y while the least was from Kathaana quarry at 0.47 ± 0.01 mSv/y. The indoor AEDR from Mavoloni Quarry was 0.52 ± 0.01 mSv/y. Kyasioni Quarry registered the highest value of 0.39 ± 0.01 mSv/y for outdoor AEDR compared to both Kathaana and Mavoloni Quarries whose values were determined as 0.32 ± 0.01 mSv/y and 0.35 ± 0.01 mSv/y respectively. Generally, the indoor AEDR was higher than the outdoor AEDR in the three quarry sample findings. This is because people spent 60 percent the day's twenty four hours indoors (Mustapha *et al*., 1999). Based on the permissible dose criterion, the use of quarry stones from Mavoloni, Kathaana and Kyasioni for building purposes poses no significant radiological hazard.

5.4 Radiation Hazard Indices

External hazard index (H_{ex}) and internal hazard index (H_{in}) were estimated by modifying radium, thorium and potassium activity concentrations using data and protocols from UNSCEAR reports. The external hazard index (H_{ex}) estimated exposure to the outermost body organs as a result of gamma radiation mainly from primordial radionuclides (^{226}Ra, ^{232}Th and ^{40}K) whereas the internal hazard index (H_{in}) estimated the exposure of internal body organs arising from inhalation of radon and thoron gases and their short-lived decay products (Tsai *et al*.,2008).

The average hazard indices associated with the three quarry construction materials is presented graphically in Figure 5.7.

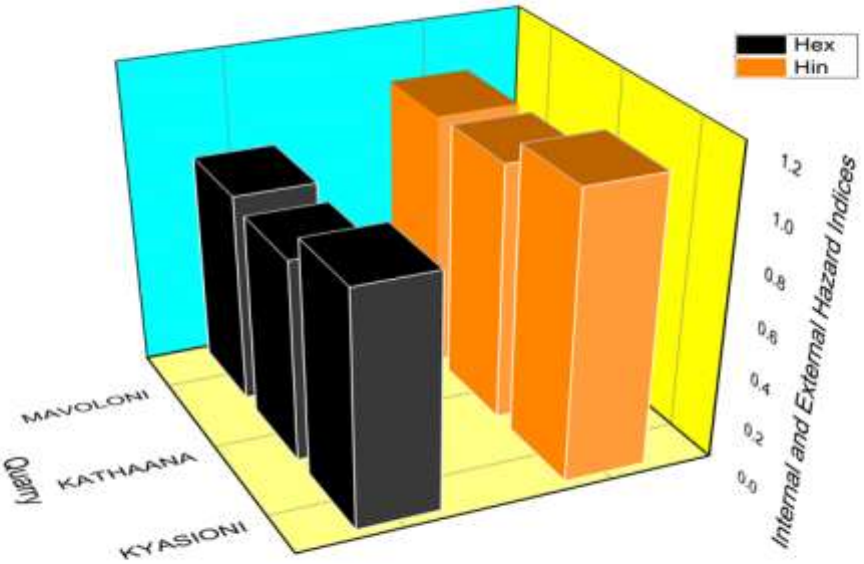

Figure 5.7: Hazard index comparison among the quarries

Samples from Kyasioni quarry registered the highest internal hazard index followed by Mavoloni and then kathaana as follows; $\mathbf{1.13 \pm 0.03, 1.01 \pm 0.03}$ and 0.92 ± 0.03. Thus, the set limit of unity is exceeded by samples from Kyasioni and Mavoloni quarries. Similarly, the external radiation hazard indices were 0.93 ± 0.02, 0.83 ± 0.02 and 0.75 ± 0.02 for Kyasioni, Mavoloni and Kathaana quarries respectively. As noted, all the values for external radiation hazard indices were relatively below the permissible value of unity (UNSCEAR, 2017). It is true from these findings that there is no major biological

effect for both internal and external hazard index from the quarries of Mavoloni and kathaana since the external hazard index from Mavoloni is in a range of error of $\pm$ 0.03 which implies that the value of 1.01 is barely within the limit. Kyasionis' internal hazard index value of 1.13 is above the permissible value of unity and therefore Quarry products from this site are radiologically unsafe based on this parameter, however, at the moment adequate house ventilation (Yarmoshenko *et al*., 2022) and further studies are highly recommended. Table 5.5 shows a summary of the radiological parameter values from this study.

Table 5.5: Summary of radiological parameter values as determined in this work

Parameter	Kyasioni	Kathaana	Mavoloni	Limit
Ra_{eq}. Activity	329.61±8.18	265.35±7.77	295.64±8.19	370 (UNSCEAR,2017)
Absorbed Dose	158.45±3.90	128.95±3.72	142.22±3.90	60 (UNSCEAR,2017)
Annual Dose $Rate_{in}$	0.58±0.01	0.47±0.01	0.52±0.01	1.2 (UNSCEAR,2017)
Annual Dose $Rate_{out}$	0.39±0.01	0.32±0.01	0.35±0.01	1.2 (UNSCEAR,2017)
Internal Hazard	**1.13±0.03**	0.92±0.03	**1.01±0.03**	1 (ICRP, 1999)
External Hazard	0.93±0.02	0.75±0.02	0.83±0.02	1 (ICRP, 1999)

5.6 Comparison of activity concentration of ^{238}U, ^{232}Th and ^{40}K from this study and other similar studies

This section presents results from various radiometric surveys carried out in Kenya and other parts of the world. The activity concentration of primordial radionuclides is either much higher than the set limits or comparable to the later or even much lower. The average activity concentration findings of ^{238}U, ^{232}Th and ^{40}K from this study was 74.75 ± 3.15 Bq/Kg, 118.48 ± 1.91 Bq/Kg and 1120.35 ± 30.07 Bq/Kg from Kyasioni quarry, 63.25 ± 3.08 Bq/Kg, 81.82 ± 1.62 Bq/Kg and 1112.55 ± 30.97 Bq/Kg from Kathaana quarry while Mavaoloni quarry site values were 67.00 ± 3.09 Bq/Kg, 105.52 ± 1.97 Bq/Kg and 1019.17 ± 29.79 Bq/Kg respectively. A quick comparison of these findings with the national mean values 28.7 Bq/Kg, 73.3 Bq/Kg and 255.7 Bq/Kg (Mustapha *et al*., 1999) for the respective natural radionuclides namely ^{238}U, ^{232}Th and ^{40}K shows that the findings from this study are a bit high. This was expected since the geology of Machakos County is made up of rocks such as limestone, amphibolites and quartzites (Dodson, 1953) which are rich in radioactive elements (Shikali, 2013). Furthermore, these concentrations have

surpassed the world's limits of 33 Bq/Kg, 45 Bq/Kg and 420 Bq/Kg for ^{238}U, ^{232}Th and ^{40}K respectively (UNSCEAR, 2017).In Table 5.6, a summary for the similarity of specific activity concentration of ^{238}U, ^{232}Th and ^{40}K from this study and earlier similar studies is given.

Table 5.6: Activity concentration (Bq/Kg) comparison from this study and other similar studies**.**

Country	**Site**	**^{226}Ra**	**^{232}Th**	**^{40}K**	**Reference**
Kenya	Kyasioni-Machakos	74.75	118.48	1120.35	Current study
Kenya	Mavoloni-Machakos	67.00	105.52	1019.17	Current study
Kenya	Kathaana-Machakos	63.25	81.52	1112.55	Current study
Kenya	Tyaa river-Kitui	21	49	782	Matsitsi *et al*., 2019
Kenya	Kibwezi District	130	137	1140	Mutie, 2011
Kenya	Kisii county	360	271.7	1780	Kinyua *et al*., 2011
Kenya	Lambwe-Western	178.69	1396.85	508.67	Achola, 2009
India	Tiruchirappali	15.5	135	859.4	Hameed *et al*., 2014
Iran	Ramsar	86400	187	1380	Sohrabi, 1993
Brazil	Quarapari	6-4100	17-47500	73-300	li, 2013
Egypt	Giza	99	211.6	106	Harb *et al*., 2012
World's average		**35**	**30**	**412**	**UNSCAER, 2000**

Graphical presentation giving further comparison for the data in Table 5.6 is shown in Figures 5.8, 5.9 and 5.10

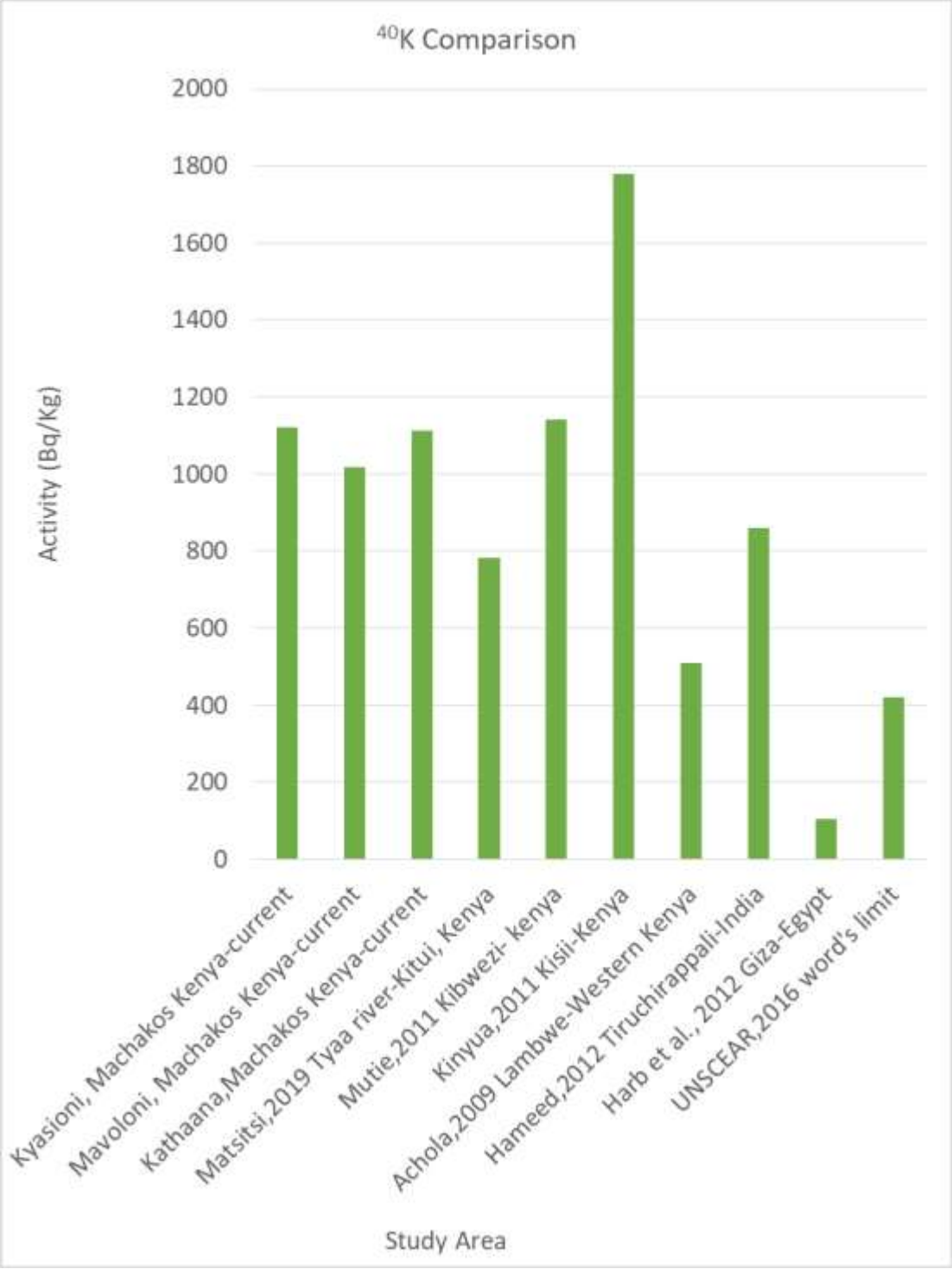

Figure 5.8: Comparison of activity concentration for ^{40}K from this study and other related studies across the world

The graphical presentation in Figure 5.8 clearly shows that the radiation activity concentration for ^{40}K radionuclide have mostly surpassed the 420 Bq/Kg set limit. This

mainly owns its' explanation from potassium's earth crusts dominancy. The ^{40}K findings from the three quarry sites under this current study are therefore not unique.

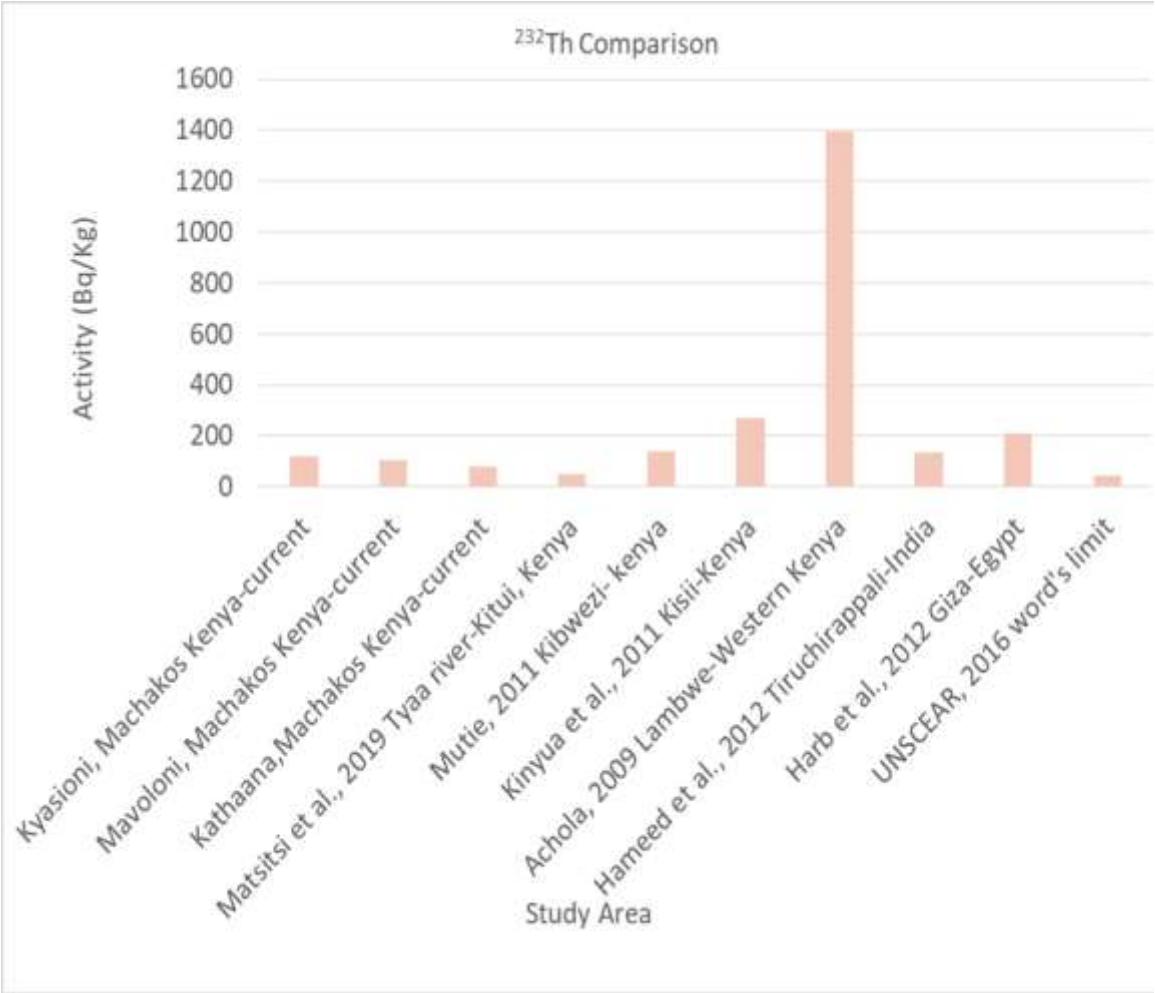

Figure 5.9: Comparison of activity concentration for ^{232}Th from this study and other related studies across the world

^{232}Th radiation activity concentration gets a perfect comparison from earlier studies as shown in Figure 5.9. Most findings giving values slightly above 100 Bq/Kg but below 300 Bq/Kg. A unique case was registered from a radiological survey in Lambwe-Western Kenya (Achola, 2009) at a value of 1396 Bq/Kg (see Table 5.6) which was beyond the limit of 45 Bq/Kg by about thirty-one times.

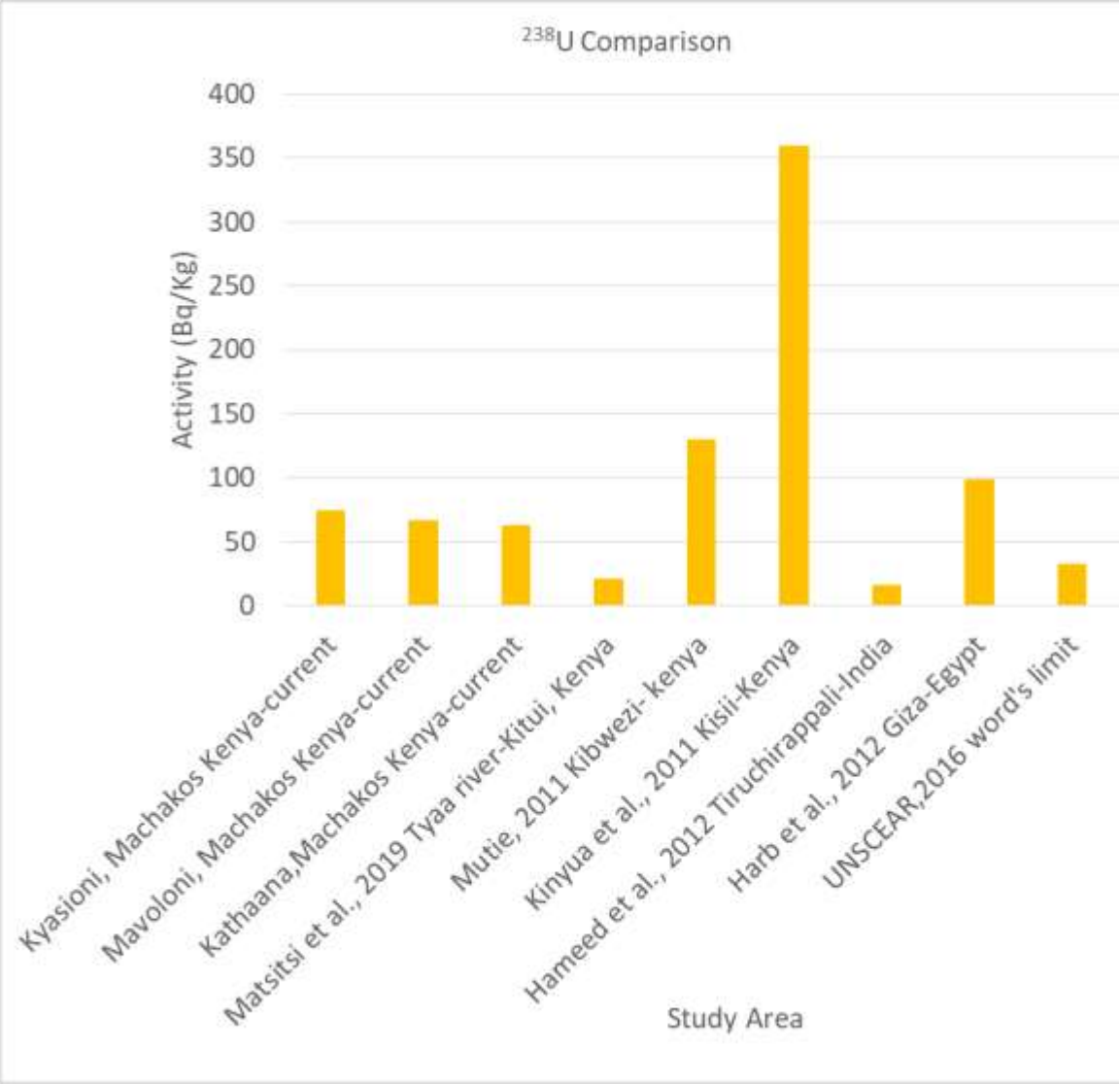

Figure 5.10: Comparison of activity concentration for ^{238}U from this study and other related studies

^{238}U activity concentration comparison in Figure 5.10 shows that the findings from this study are similar to earlier outcomes from other related studies. Most findings are observed as below 100 Bq/Kg but above the word's average of 33 Bq/Kg however, some elevated values are noted. As evident from this work, elevated levels of radiation activity

concentration of the radionuclides of ^{40}K, ^{232}Th, and ^{238}U do not necessarily lead to dosimetric values that surpass the permissible limits although it's always a cause of alarm when their values are extremely high.

CHAPTER SIX

CONCLUSIONS AND RECOMMENDATIONS

6.1 Conclusions

The radiological parameters of rocks from the three selected quarries in Machakos County were determined. The average activities of the NORM, namely ^{40}K, ^{238}U, and ^{232}Th were computed from activities of 14 samples from each quarry and were found to be beyond the permissible limits of 420 Bq/kg, 33 Bq/kg, and 45 Bq/Kg respectively (UNSCAER, 2017). Since the other radiological parameters are derived from the activity concentration, it was expected that there may be some dosimetric parameters having elevated values as well. As a result, the contribution of NORM to the internal hazard index from Kyasioni and Mavoloni quarries revealed that they surpassed the safety limit by about 0.13 and 0.01 respectively. These values are somehow alarming although their impact is highly neutralized through proper house ventilation (Yarmoshenko *et al.*, 2022). Furthermore, internal hazard index being the only parameter that was surpassed, its cumulative effect might not be radiologically dangerous. The value for the internal hazard index from Kathaana quarry was slightly lower than the set limit as it stood at 0.92. All the calculated values for the external hazard index were found to be below the set limit of unity. Both values of indoor and outdoor annual effective dose rates were below the safety limit of 1.2.

On average, although the three quarries registered several values just below the recommended limits for the radiological parameters examined, values from Kyasioni quarry were relatively higher compared to those of other quarries. One radiological parameter (internal radiation hazard index) was beyond the permissible limit for Kyasioni and Mavoloni quarry sample materials. Kathaana quarry sample materials did not surpass any of the radiological parameters examined. Since most of the radiological dosimetric parameter limits were not exceeded, this study concludes that building and construction rocks from the three quarries are safe for the said purposes. Moreover, building rocks from Kathaana quarry pose the lowest radiological risks. At the same time, rocks from Kyasioni and Mavoloni pose some radiological risk although somehow insignificant.

6.2 Recommendations

The demand for building and construction materials remains very high as the real estate industry and infrastructure is rapidly growing in Kenya. However, dwelling in structures that may expose occupants to radiological risks can be avoided through the following suggestions on sourcing construction materials.

1. It is strongly recommended that a further radiological study would be necessary to re-examine the radiological parameter values in the studied area.
2. A current geological study should be carried out in this area to ascertain the type of rocks in these quarries
3. As this study randomly selected samples from the quarries and did not consider the soils and rocks in the neighborhood, it is recommended that a future study could be done on those materials to compare with the radioactivity of the materials from the quarries.
4. This study also recommends an onsite assessment of radon in the air to assess the dose levels of personnel working in the mines.

REFERENCES

Achola, S. O. (2009). *Radioactivity and elemental analysis of carbonatite rocks from parts of Gwasi area, South Western Kenya* (Doctoral dissertation, University of NAIROBI).

Ahad, A., ur Rehman, S., ur Rehman, S., & Faheem, M. (2004). Measurement of radioactivity in the soil of Bahawalpur division, Pakistan. *Radiation Protection Dosimetry*, *112*(3), 443-447.

Allen, C., Borak, T. B., Tsujii, H., & Nickoloff, J. A. (2011). Heavy charged particle radiobiology: using enhanced biological effectiveness and improved beam focusing to advance cancer therapy. *Mutation Research/Fundamental and Molecular Mechanisms of Mutagenesis*, *711*(1-2), 150-157.

Alam, M., Rais, S., & Aslam, M. (2012). Hydrochemical investigation and quality assessment of ground water in rural areas of Delhi, India. *Environmental Earth Sciences*, *66*, 97-110.

Alnour, I. A., Wagiran, H., Ibrahim, N., Laili, Z., Omar, M., Hamzah, S., & Idi, B. Y. (2012). Natural radioactivity measurements in the granite rock of quarry sites, Johor, Malaysia. *Radiation Physics and Chemistry*, *81*(12), 1842-1847.

Alencar, A. S., & Freitas, A. C. (2005). Reference levels of natural radioactivity for the beach sands in a Brazilian southeastern coastal region. *Radiation Measurements*, *40*(1), 76-83.

Almeida, R. M., Lauria, D. C., Ferreira, A. C., & Sracek, O. (2004). Groundwater radon, radium and uranium concentrations in Regiao dos Lagos, Rio de Janeiro State, Brazil. *Journal of Environmental Radioactivity*, *73*(3), 323-334.

Al-Zahrani, J. H. (2017). Estimation of natural radioactivity in local and imported polished granite used as building materials in Saudi Arabia. *Journal of radiation research and applied sciences*, *10*(3), 241-245.

Andreo, P., Burns, D. T., Nahum, A. E., Seuntjens, J., & Attix, F. H. (2017). *Fundamentals of ionizing radiation dosimetry*. John Wiley & Sons.

Arthur, M. D., Brysk, H., Paveri-Fontana, S. L., & Zweifel, P. F. (1981). Law of radioactive decay. *Nuovo Cimento B;(Italy)*, *63*(2).

Bala, R., Das, D., Naskar, N., & Lahiri, S. (2022). Vertical distribution and radiological risk assessment of natural radionuclides in the alluvial soil profile of south-west Punjab, India. *Journal of Radioanalytical and Nuclear Chemistry*, *331*(6), 2561-2572.

Benke, R. R., & Kearfott, K. J. (1999). Soil sample moisture content as a function of time during oven drying for gamma-ray spectroscopic measurements. *Nuclear Instruments and Methods in Physics Research Section A: Accelerators, Spectrometers, Detectors and Associated Equipment*, *422*(1-3), 817-819.

Beretka, J., & Mathew, P. J. (1985). Natural radioactivity of Australian building materials, industrial wastes and by-products. *Health physics*, *48*(1), 87-95.

Bobbo, M. O., Ii, J. E. N. N., Suzuki, T., Kudo, H., Hosoda, M., Owono, L. C. O., & Tokonami, S. (2019). Occupational Natural Radiation Exposure at the Uranium Deposit of Kitongo, Cameroon. *Radioisotopes*, *68*(9), 621-630.

Bohm, G., & Zech, G. (2014). Statistics of weighted Poisson events and its applications. *Nuclear Instruments and Methods in Physics Research Section A: Accelerators, Spectrometers, Detectors and Associated Equipment*, *748*, 1-6.

Brodsky, A. (1978). *CRC Handbook of radiation measurement and protection*. Crc Press.

Britannica, E. (2021). Available online: https://www. britannica. com/science. *Geophone (accessed on 10 March 2021)*.

Brynjolfsson, A. (2002). *Natural and induced radioactivity in food* (Vol. 1287). International Atomic Energy Agency, IAEA.

Bucher, K., & Frey, M. (2002). *Petrogenesis of metamorphic rocks*. Springer Science & Business Media.

Bushberg, J. T., & Boone, J. M. (2011). *The essential physics of medical imaging*. Lippincott Williams & Wilkins.

Clarke, R. H. (1992). Work of ICRP Committee 4. *Radiological Protection Bulletin;(United Kingdom)*, *134*.

Crouthamel, C. E., Adams, F., & Dams, R. (2013). *Applied gamma-ray spectrometry* (Vol. 41). Elsevier.

Desouky O. and Nan Din (2015). Targeted and non-targeted effects of ionizing radiation. *Journal of radiation research and applied sciences-pp3*

Diehl, J. F. (1999). *Safety of irradiated foods*. CRC Press.

Dodson, R. G. (1953). *Geology of the south-east Machakos area: degree sheet 52, SE quadrant (with coloured map)* (No. 25). Government Printer.

Donnelly, K. E., Goldstein, S. L., Langmuir, C. H., & Spiegelman, M. (2004). Origin of enriched ocean ridge basalts and implications for mantle dynamics. *Earth and Planetary Science Letters*, *226*(3-4), 347-366.

Ebaid, Y. Y. (2010). Use of gamma-ray spectrometry for uranium isotopic analysis in environmental samples. *Rom J phys*, *55*(1-2), 69-74.

Eberth, J., & Simpson, J. (2008). From Ge (Li) detectors to gamma-ray tracking arrays–50 years of gamma spectroscopy with germanium detectors. *Progress in Particle and Nuclear Physics*, *60*(2), 283-337.

Eisenbud, M., & Gesell, T. F. (1997). *Environmental radioactivity from natural, industrial and military sources: from natural, industrial and military sources*. Elsevier.

El-Gamal, A., Nasr, S., & El-Taher, A. (2007). Study of the spatial distribution of natural radioactivity in the upper Egypt Nile River sediments. *Radiation measurements*, *42*(3), 457-465.

Enoh, M. A., Njoku, R. E., & Okeke, U. C. (2022). Modeling and mapping the spatial–temporal changes in land use and land cover in Lagos: A dynamics for building a sustainable urban city. *Advances in Space Research*.

Fairburn, W. A. (1963). Geology of the north Machakos-Thika area. *Rept. Geol. Surv. Kenya*, *59*.

Fisher, D. R., & Fahey, F. H. (2017). Appropriate use of effective dose in radiation protection and risk assessment. *Health physics*, *113*(2), 102.

Gao, G. Q. (2003). *Computerised detection and classification of five cardiac conditions* (Doctoral dissertation, Auckland University of Technology).

Ghiassi-Nejad, M., Mortazavi, S. M. J., Cameron, J. R., Niroomand-Rad, A., & Karam, P. A. (2002). Very high background radiation areas of Ramsar, Iran: preliminary biological studies. *Health physics*, *82*(1), 87-93.

Gilmore, G. (2008). *Practical gamma-ray spectroscopy*. John Wiley & Sons.

Goldsten, J. O., Rhodes, E. A., Boynton, W. V., Feldman, W. C., Lawrence, D. J., Trombka, J. I., ... & Witte, M. C. (2007). The MESSENGER gamma-ray and neutron spectrometer. *The Messenger Mission to Mercury*, 339-391.

Hameed, P. S., Pillai, G. S., Satheeshkumar, G., & Mathiyarasu, R. (2014). Measurement of gamma radiation from rocks used as building material in Tiruchirappalli district, Tamil Nadu, India. *Journal of Radioanalytical and Nuclear Chemistry*, *300*, 1081-1088.

Harb, S. R. M. (2004). On the human radiation exposure as derived from the analysis of natural and man-made radionuclides in soils.

Harb, S., Abbady, A. E. B., El-Kamel, A. E. H., Saleh, I. I., & Abd El-Mageed, A. I. (2012). Natural radioactivity and their radiological effects for different types of rocks from Egypt. *Radiation Physics and Chemistry*, *81*(3), 221-225.

Harrison, J. D., & Streffer, C. (2007). The ICRP protection quantities, equivalent and effective dose: their basis and application. *Radiation protection dosimetry*, *127*(1-4), 12-18.

Heinrich, W., Roesler, S., & Schraube, H. (1999). Physics of cosmic radiation fields. *Radiation protection dosimetry*, *86*(4), 253-258

Hietanen, M. (2006). Health risks of exposure to non-ionizing radiation-Myths or science-based evidence. *Medicina Del Lavoro*, *97*(2), 184.

IAEA. (2004). Soil sampling for environmental contaminants. *IAEA Tec-Doc-1415*.

International Commission on Radiological Protection. (1999). *Protection of the Public in Situations of Prolonged Radiation Exposure: The Application of the Commission's System of Radiological Protection to Controllable Radiation Exposure Due to Natural Sources and Long-lived Radioactive Residues*. Pergamon for the International Commission on Radiological Protection.

International Commission on Non-Ionizing Radiation Protection. (2020). Guidelines for limiting exposure to electromagnetic fields (100 kHz to 300 GHz). *Health physics*, *118*(5), 483-524.

Joshua, E. O., Ademola, J. A., Akpanowo, M. A., Oyebanjo, O. A., & Olorode, D. O. (2009). Natural radionuclides and hazards of rock samples collected from Southeastern Nigeria. *Radiation measurements*, *44*(4), 401-404.

Karbownik, M., & Reiter, R. J. (2000). Antioxidative effects of melatonin in protection against cellular damage caused by ionizing radiation (44547). *Proceedings of the Society for Experimental Biology and Medicine*, *225*(1), 9-22.

Kaur, R., Shikha, D., Kaushal, A., Gupta, R., Singh, S. P., Chauhan, R. P., & Mehta, V. (2021). Measurement of indoor 222 Rn, 220 Rn and decay products along with naturally occurring radionuclides in some monuments and museums of Punjab, India. *Journal of Radioanalytical and Nuclear Chemistry*, *330*, 1357-1364.

Kavasi, N. J.Somlai, G. Szeiler, B. Szabo, I. Schafer, T. Kovacs. (2010). Estimation of effective doses to cavers based on radon measurements carried out in seven caves of the Bacony Mountains in Hungary. *Radiation measurements*, 45(2010), pp. 1068-1071.

Kendall, C., & Caldwell, E. A. (1998). Fundamentals of isotope geochemistry. In *Isotope tracers in catchment hydrology* (pp. 51-86). Elsevier.

Kinyua, R., Atambo, V. O., & Ongeri, R. M. (2011). Activity concentrations of 40K, 232Th, 226Ra and radiation exposure levels in the Tabaka soapstone quarries of the Kisii Region, Kenya. *African journal of environmental science and Technology*, *5*(9), 682-688.

Khan, F. M., & Gibbons, J. P. (2014). *Khan's the physics of radiation therapy*. Lippincott Williams & Wilkins.

Knipp, J. K., & Uhlenbeck, G. E. (1936). Emission of gamma radiation during the beta decay of nuclei. *Physica*, *3*(6), 425-439.

Knoll, G. F. (2010). *Radiation detection and measurement*. John Wiley & Sons.

Kudriashov, I. B., & Kudriashov, Y. B. (2008). *Radiation Biophysics (Ionizing Radiations)*. Nova Publishers.

Kumar, A., Sharma, S., Mehra, R., Narang, S., & Mishra, R. (2017). Assessment of indoor radon, thoron concentrations, and their relationship with seasonal variation and geology of Udhampur district, Jammu & Kashmir, India. *International journal of occupational and environmental health*, *23*(3), 202-214.

Lakshmi, K. S., Selvasekarapandian, S., Khanna, D., and Meenakshisundaram, V. (2005). Primordial radionuclides concentrations in the beach sands of East Coast region of Tamilnadu, India. *In International Congress Series* (Vol. 1276, pp. 323-324). Elsevier.

Lecoq, P. (2020). Scintillation detectors for charged particles and photons. *Particle Physics Reference Library: Volume 2: Detectors for Particles and Radiation*, 45-89.

Leo, W. R. (2012). *Techniques for nuclear and particle physics experiments: a how-to approach*. Springer Science & Business Media.

Liao, Y. (2006). Practical electron microscopy and database. *An Online Book*.

Lieser, K. H. (2008). *Nuclear and radiochemistry: fundamentals and applications*. John Wiley & Sons.

Litvinenko, A., Iurchuk, V., Sethi, P., Louis, S., Tyberkevych, V., Li, J., ... & Ebels, U. (2020). Ultrafast sweep-tuned spectrum analyzer with temporal resolution based on a spin-torque nano-oscillator. *Nano letters*, *20*(8), 6104-6111.

Liu, X., & Lin, W. (2018). Natural radioactivity in the beach sand and soil along the coastline of Guangxi Province, China. *Marine pollution bulletin*, *135*, 446-450.

Li, W., Mahadevan, V., & Vasconcelos, N. (2013). Anomaly detection and localization in crowded scenes. *IEEE transactions on pattern analysis and machine intelligence*, *36*(1), 18-32.

Mahur, A. K., Kumar, R., Sonkawade, R. G., Sengupta, D., & Prasad, R. (2008). Measurement of natural radioactivity and radon exhalation rate from rock samples of Jaduguda uranium mines and its radiological implications. *Nuclear Instruments and Methods in Physics Research Section B: Beam Interactions with Materials and Atoms*, *266*(8), 1591-1597.

Mahuvava, C., & Du Plessis, F. C. P. (2015). Monte Carlo evaluation of the dose perturbation effect of hip prostheses for megavoltage photon radiotherapy. *Physica Medica: European Journal of Medical Physics*, *31*, S7.

Malik, S. S., & Gupta, R. K. (1989). Theory of cluster radioactive decay and of cluster formation in nuclei. *Physical Review C*, *39*(5), 1992.

Mangala, J. M. (1987). *A multichannel X-ray fluorescence analyses of fluorspar ore and rocks from Mrima hills, Kenya* (Doctoral dissertation, Msc thesis. University of Nairobi).

Manohara, S. R., & Hanagodimath, S. M. (2007). *and Methods in Physics Research Section B: Beam Interactions with Materials and Atoms*, *258*(2), 321-328.

Matsitsi, S. M., Linturi, J. M., Kebwaro, J. M., & Maweu, O. M. (2019). Effects of Seasonal Change on the Levels of Geogenic Radionuclides in Sand and Rocks from Tyaa River deposit in Kitui County: Geophysics. *International Journal of Fundamental Physical Sciences*, *9*(1), 14-19.

Mba, C., Afza, R., & Shu, Q. Y. (2012). Mutagenic radiations: X-rays, ionizing particles and ultraviolet. In *Plant mutation breeding and biotechnology* (pp. 83-90). Wallingford UK: CABI.

Mbuzukongira, P. (2006). *Assessment of occupational radiation exposures of artisan miners of columbite-tantalite (coltan) in the Eastern democratic republic of Congo* (Doctoral dissertation).

McCollough, C. H., & Schueler, B. A. (2000). Calculation of effective dose. *Medical physics*, *27*(5), 828-837.

Michaud, A. (2013). The Mechanics of Electron-Positron Pair Creation in the 3-Spaces Model. *International Journal of Engineering Research and Development, e-ISSN*, 36-49.

Mulwa, B. M., Maina, D. M., & Patel, J. P. (2013). Radiological analysis of suitability of Kitui South limestone for use as building material. *International Journal of Fundamental Physical Sciences (IJFPS)*, *3*(2), 32-35.

Mustapha, A. O., Patel, J. P., & Rathore, I. V. S. (1999). Assessment of human exposures to natural sources of radiation in Kenya. *Radiation protection dosimetry*, *82*(4), 285-292.

Mutie, M.M. (2011). Measurement of the elemental and radionuclide concentrations of environmental and geological samples from selected ares of Kibwezi District, Kenya. M.Sc.(Physics) thesis Kenyatta University, Kenya. pp 49-50.

Nations, U. (2000). Basic facts: About the United Nations. *New York: United Nations publication*.

Nelson, G., & Reilly, D. (1991). Gamma-ray interactions with matter. *Passive nondestructive analysis of nuclear materials*, *2*, 27-42.

OCW, M. (2008). Mit opencourseware. *from Wikipedia, the free encyclopedia. http://en. wikipedia. org/wiki/MIT_OpenCourseWare*.

Otwoma, D., J. P. Patel, S. Bartilol, and A. O. Mustapha. "Estimation of annual effective dose and radiation hazards due to natural radionuclides in mount Homa, southwestern Kenya." *Radiation protection dosimetry* 155, no. 4 (2013): 497-504.

Papadopoulos, A., Christofides, G., Koroneos, A., Papadopoulou, L., Papastefanou, C., & Stoulos,

S. (2013). Natural radioactivity and radiation index of the major plutonic bodies in Greece. *Journal of Environmental Radioactivity*, *124*, 227-238.

Paquet, F., Bailey, M. R., Leggett, R. W., Lipsztein, J., Marsh, J., Fell, T. P., & Harrison, J. D. (2017). ICRP publication 137: occupational intakes of radionuclides: part 3. *Annals of the ICRP*, *46*(3-4), 1-486.

Podgorsak, E. B. (2005). *Radiation oncology physics*. Vienna: IAEA.

Protection, R. (2007). ICRP publication 103. *Ann ICRP*, *37*(2.4), 2.

Pulfrey, W. (1960). *Shape of the sub-Miocene erosion bevel in Kenya* (Vol. 3). Government Printer.

Rasheed, A. A., Kadhum, N. F., & Ibrahim, N. K. (2016). Natural radioactivity and associated dose rates in soil samples in the destroyed fuel fabrication facility, Iraq. *International Journal of Physics*, *4*(3), 50-54.

Reguigui, N. (2006). Gamma ray spectrometry. *Practical Information*, *21*.

Riley, P. A. (1994). Free radicals in biology: oxidative stress and the effects of ionizing radiation. *International journal of radiation biology*, *65*(1), 27-33.

Rittersdorf, I. (2007). Gamma ray spectroscopy. *Nuclear Engineering & Radiological Sciences*, 18-20.

Rösch, F., & Knapp, F. F. (2011). Radionuclide generators. In *Handbook of nuclear chemistry* (pp. 1935-1976). Springer, Boston, MA.

Saha, G. B., & Saha, G. B. (2004). *Fundamentals of nuclear pharmacy* (Vol. 6, pp. 96-100). New York: Springer.

Scheinman, L. (2016). *The international atomic energy agency and world nuclear order*. Routledge.

Schmid, T. E., Dollinger, G., Hable, V., Greubel, C., Zlobinskaya, O., Michalski, D., & Röper, B. (2010). Relative biological effectiveness of pulsed and continuous 20 MeV protons for micronucleus induction in 3D human reconstructed skin tissue. *Radiotherapy and Oncology*, *95*(1), 66-72.

Seibert, J. A. (2004). X-ray imaging physics for nuclear medicine technologists. Part 1: Basic principles of x-ray production. *Journal of nuclear medicine technology*, *32*(3), 139-147.

Sempau, J., Fernández-Varea, J. M., Acosta, E., & Salvat, F. (2003). Experimental benchmarks of the Monte Carlo code PENELOPE. *Nuclear Instruments and Methods in Physics Research Section B: Beam Interactions with Materials and Atoms*, *207*(2), 107-123.

Seuntjens, J. P., Strydom, W. Y. N. A. N. D., & Shortt, K. R. (2005). Dosimetric principles, quantities and units. *Radiation oncology physics: a handbook for teachers and students. Podgorsak EB, editor. Vienna, Austria: IAEA.*

Shikali, N. C. (2013). Radionuclide content of sand used for construction in Kakamega County and associated indoor radon diffusion doses.

Siegbahn, K. (Ed.). (2012). *Alpha-, beta-and gamma-ray spectroscopy*. Elsevier.

Sohrabi, M. (1993, August). Recent radiological studies of high level natural radiation areas of Ramsar. In *Proceeding of International Conference on High Levels of Natural Radiations* (Vol. 3, No. 7, pp. 39-47).

Sohrabi, M. (1998). The state-of-the-art on worldwide studies in some environments with elevated naturally occurring radioactive materials (NORM). *Applied Radiation and Isotopes*, *49*(3), 169-188.

Tricot, N., Chellapandi, P., Reitsma, F., & Tuček, K. (2013). IAEA Safety Standards for Fast Neutron Reactors and High Temperature Gas-cooled Reactors.

Tsai, T. L., Lin, C. C., Wang, T. W., & Chu, T. C. (2008). Radioactivity concentrations and dose assessment for soil samples around nuclear power plant IV in Taiwan. *Journal of radiological protection*, *28*(3), 347.

Tzortzis, M., Svoukis, E., & Tsertos, H. (2004). A comprehensive study of natural gamma radioactivity levels and associated dose rates from surface soils in Cyprus. *Radiation protection dosimetry*, *109*(3), 217-224.

United Nations Scientific Committee on the Effects of Atomic Radiation. (2017). *Sources, effects and risks of ionizing radiation, united nations scientific committee on the effects of atomic radiation (UNSCEAR) 2016 report: report to the general assembly, with scientific annexes*. United Nations.

Unscear, S. (2000). Effects of Ionizing Radiation. *United Nations, New York*, 453-487.

United Nations Scientific Committee on the Effects of Atomic Radiation. (2010). *Sources and Effects of Ionizing Radiation, United Nations Scientific Committee on the Effects of Atomic Radiation (UNSCEAR) 2008 Report, Volume I: Report to the General Assembly, with Scientific Annexes A and B-Sources*. United Nations.

Urbain, W. (2012). *Food irradiation*. Elsevier.

Valentin, J. (2002). Basic anatomical and physiological data for use in radiological protection: reference values: ICRP Publication 89: Approved by the Commission in September 2001. *Annals of the ICRP*, *32*(3-4), 1-277.

Valentin, J. (2005). Low-dose extrapolation of radiation-related cancer risk. *Annals of the ICRP*, *35*(4), 1-140.

Valentin, J. (2007). *The 2007 recommendations of the international commission on radiological protection* (Vol. 37, No. 2-4, pp. 1-133). Oxford: Elsevier.

Valko, M., Leibfritz, D., Moncol, J., Cronin, M. T., Mazur, M., & Telser, J. (2007). Free radicals and antioxidants in normal physiological functions and human disease. *The international journal of biochemistry & cell biology*, *39*(1), 44-84.

Vanmarcke, H. (2002). UNsCEAR 2000: sources of ionizing radiation. *Annalen van de Belgische vereniging voor stralingsbescherming*, *27*(2), 41-65.

Venugopal, V., & Bhagdikar, P. S. (2012). de Broglie Wavelength and Frequency of the Scattered Electrons in Compton Effect. *arXiv preprint arXiv:1202.4572*.

Veiga, R., Sanches, N., Anjos, R. M., Macario, K., Bastos, J., Iguatemy, M., ... & Umisedo, N. K. (2006). Measurement of natural radioactivity in Brazilian beach sands. *Radiation measurements*, *41*(2), 189-196.

Wang, W. H. (2003). The operational characteristics of a sodium iodide scintillation counting system as a single-channel analyzer. *Radiation protection management*, *20*(5), 28-36.

Ward, J. F. (1988). DNA damage produced by ionizing radiation in mammalian cells: identities, mechanisms of formation, and reparability. *Progress in nucleic acid research and molecular biology*, *35*, 95-125.

Weber, W. J. (1988). Radiation effects in nuclear waste glasses. *Nuclear Instruments and Methods in Physics Research Section B: Beam Interactions with Materials and Atoms*, *32*(1-4), 471-479.

Yang, J., Koller, G. J., Fares, C., Ren, F., Pearton, S. J., Bae, J., & Smith, D. J. (2019). 60Co gamma ray damage in homoepitaxial β-Ga2O3 Schottky rectifiers. *ECS Journal of Solid State Science and Technology*, *8*(7), Q3041.

Yarmoshenko, I. V., Onishchenko, A. D., Malinovsky, G. P., Vasilyev, A. V., & Zhukovsky, M. V. (2022). MODELING and justification of indoor radon prevention and remediation measures in multi-storey apartment buildings. *Results in Engineering*, *16*, 100754.

APPENDIX 1

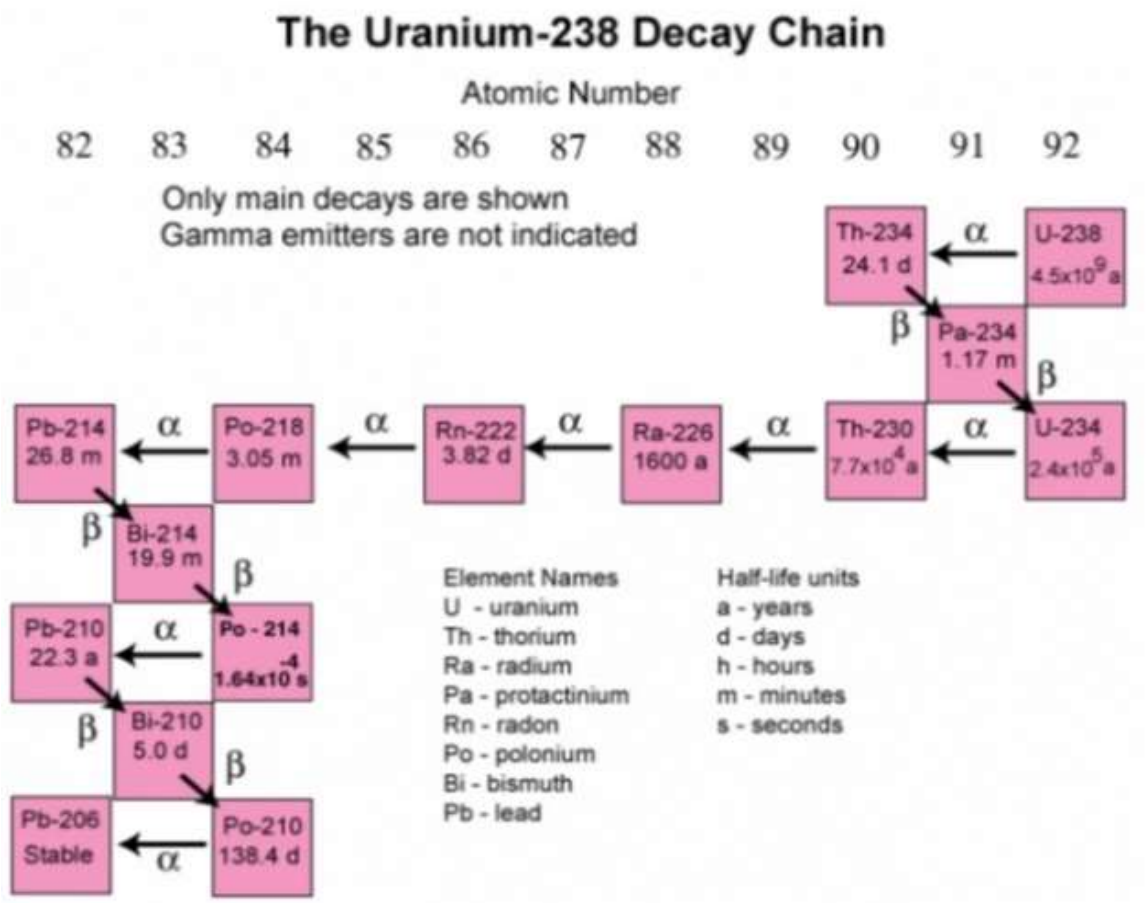

Figure A1: Uranium-238 decay chain (USEPA, 2021)

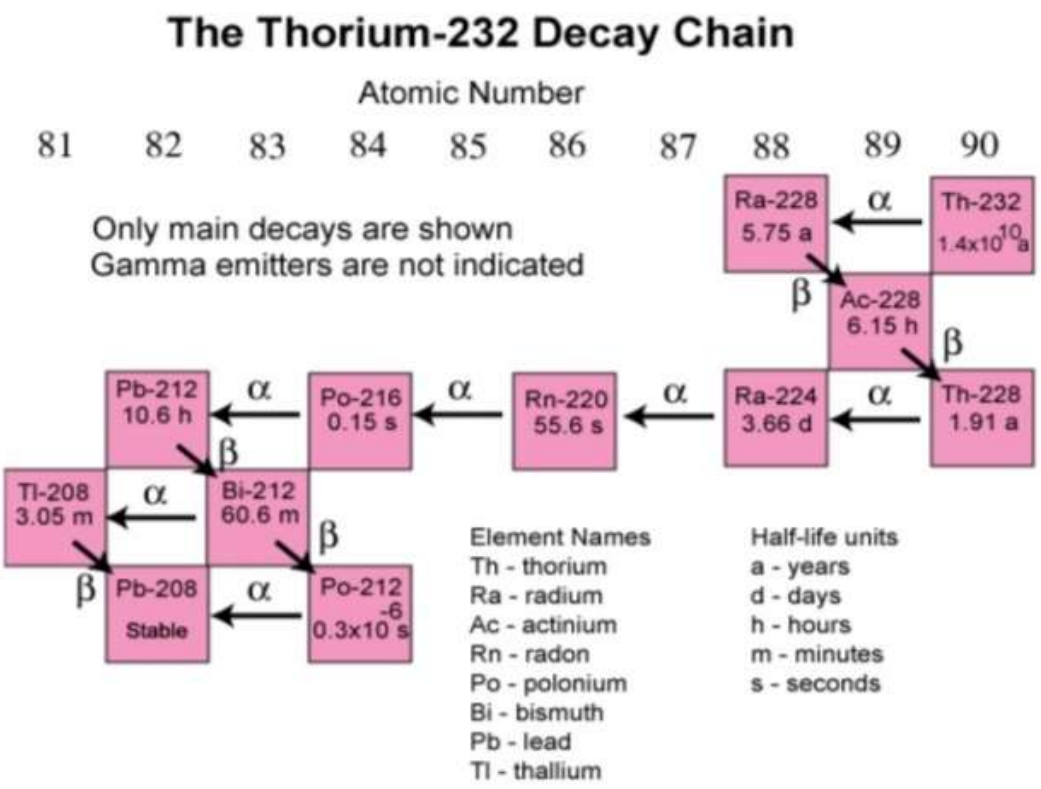

Figure A2: Thorium-232 decay chain (USEPA, 2021)

APPENDIX 3

Figure A3: Miners at work in Kathaana Quarry

APPENDIX 4

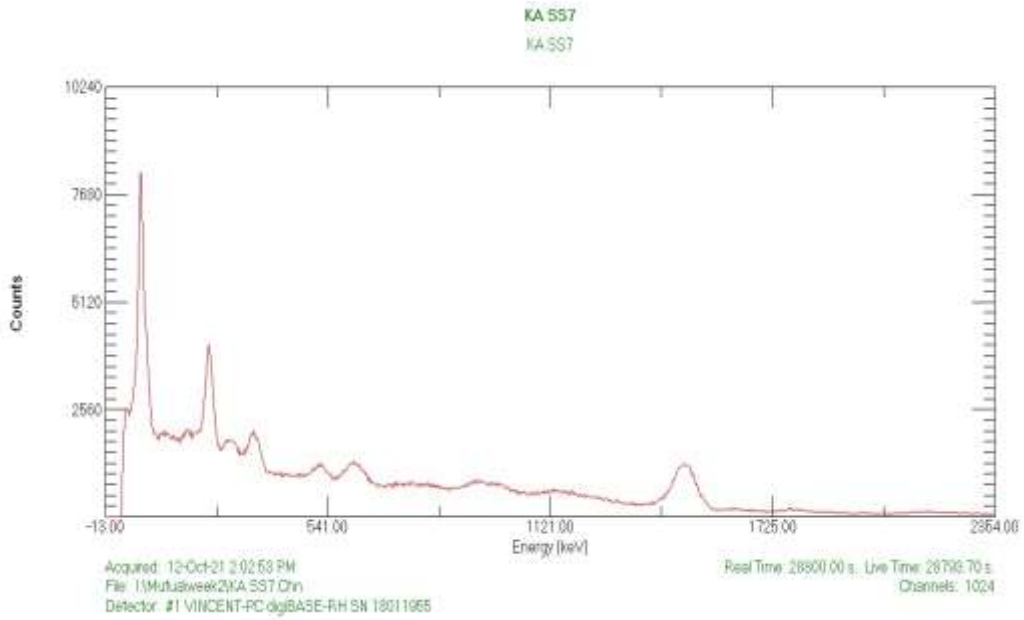

Figure A4: Kathaanas' sample seven spectrum

APPENDIX 5

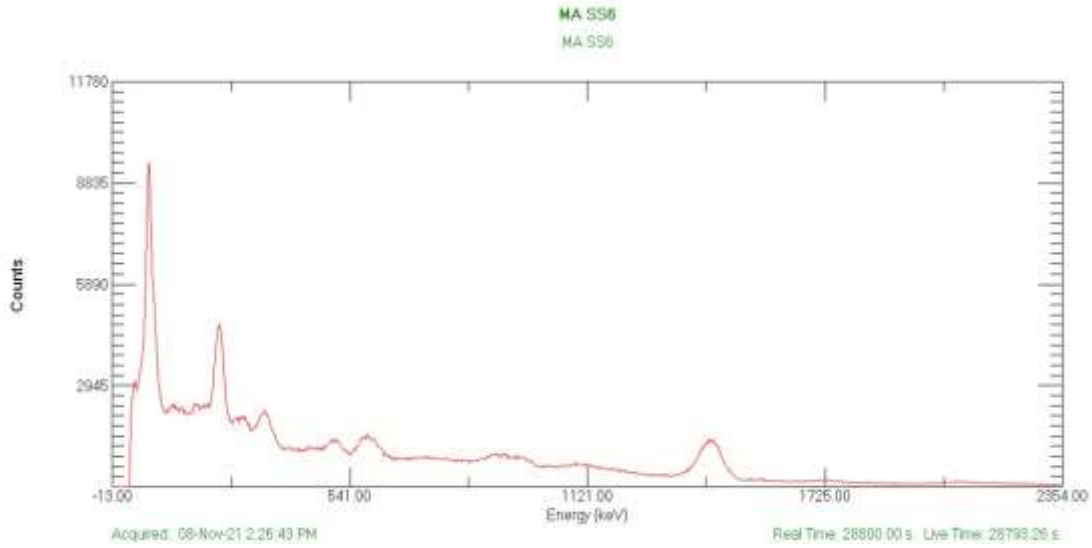

Figure A5: Mavolonis' sample six spectrum